JOURNAL OF GEOPHYSICAL RESEARCH, VOL. 107, NO. D10, 10.1029/2001JD000694, 2002

Atmospheric budget of acetone

Daniel J. Jacob, Brendan D. Field, Emily M. Jin, Isabelle Bey, Qinbin Li,
Jennifer A. Logan, and Robert M. Yantosca

Division of Engineering and Applied Sciences and Department of Earth and Planetary Sciences, Harvard University, Cambridge, Massachusetts, USA

Hanwant B. Singh

NASA Ames Research Center, Moffett Field, California, USA

Received 29 March 2001; revised 18 September 2001; accepted 21 September 2001; published 30 May 2002.

[1] The atmospheric budget and distribution of acetone are investigated by using a priori estimates of sources and sinks to constrain a global three-dimensional atmospheric model simulation and then using atmospheric observations from 14 surface sites and 5 aircraft missions to improve these estimates through an inversion analysis. Observations over the South Pacific imply a large photochemical marine source of acetone, either from the ocean or from marine organic aerosol. Low concentrations of acetone measured at European sites in winter-spring and in the Arctic in summer suggest a large microbial ocean sink. The summer-to-fall decrease of concentrations observed in Europe argues against a large source from plant decay. Continental observations in the tropics and at northern midlatitudes in summer imply a large source from terrestrial vegetation. Observations in the Northern Hemisphere outside summer imply a large source from atmospheric oxidation of anthropogenic isoalkanes (propane, isobutane, isopentane). Model simulation of isoalkanes and comparison to observations yields best global emission estimates of 12 Tg C yr^{-1} for propane (including only 0.6 Tg C yr^{-1} from biomass burning), 3.6 Tg C yr^{-1} for isobutane, and 5.0 Tg C yr^{-1} for isopentane. Our best estimate of the global acetone source is 95 Tg yr^{-1}. The mean tropospheric lifetime of acetone is estimated to be 15 days. Terrestrial vegetation and oceans are the principal sources of acetone in the tropopause region (0.1–0.7 ppbv) except in the extratropical Northern Hemisphere, where oxidation of isoalkanes is more important. *INDEX TERMS:* 0322 Atmospheric Composition and Structure: Constituent sources and sinks; 0312 Atmospheric Composition and Structure: Air/sea constituent fluxes (3339, 4504); 0315 Atmospheric Composition and Structure: Biosphere/atmosphere interactions; 0365 Atmospheric Composition and Structure: Troposphere—composition and chemistry; *KEYWORDS:* Acetone, tropospheric chemistry, propane, inverse modeling, sea-air exchange, biosphere-atmosphere interactions

1. Introduction

[2] Acetone is present ubiquitously in the troposphere at concentrations in the range 0.2–3 ppbv [*Singh et al.*, 1994, 1995, 2000, 2001; *Arnold et al.*, 1997; *Wohlfrom et al.*, 1999]. Photolysis of acetone in the upper troposphere is a major source of hydrogen oxide radicals (HO_x = OH + peroxy radicals) and peroxyacetylnitrate (PAN), with important implications for global tropospheric chemistry [*Singh et al.*, 1995; *Jaeglé et al.*, 1997, 2001; *McKeen et al.*, 1997; *Wennberg et al.*, 1998; *Collins et al.*, 1999; *Müller and Brasseur*, 1999]. The sources of acetone are poorly understood, as illustrated by the range of literature estimates in Table 1. Sinks include photolysis and reaction with OH, resulting in a global mean lifetime for acetone of the order of a month [*Gierczak et al.*, 1998]. Deposition to land and oceans has been proposed as an additional sink [*Chatfield et al.*, 1987; *Singh et al.*, 1994]. Atmospheric measurements of acetone concentrations have been made at a number of surface sites and during aircraft campaigns over the past decade (Table 2). In the present paper we use a global three-dimensional (3-D) model simulation to examine the consistency between these atmospheric measurements and our current understanding of acetone sources and sinks. Several global 3-D model studies of tropospheric chemistry have previously compared simulated and observed acetone concentrations as part of their general model evaluation [*Hauglustaine et al.*, 1998; it *Wang et al.*, 1998b; *Collins et al.*, 1999], but they used only a few observational data sets and did not interpret results in detail. We present here a more comprehensive analysis.

0148-0227/02/2001JD000694$09.00

2. Model Description

2.1. Framework

[3] We use the GEOS-CHEM global 3-D model of tropospheric chemistry [*Bey et al.*, 2001] as a forward model to simulate the atmospheric distributions of acetone and its precursors. The model uses assimilated meteorological observations from the NASA Goddard Earth Observing System (GEOS) including winds, convective mass fluxes, mixed layer depths, temperature, cloud optical depths, and surface properties. We use meteorological data for 1993–1994 available with 3- to 6-hour temporal resolution, 2° latitude × 2.5° longitude horizontal resolution, and 20 vertical sigma levels up to 10 hPa. The four lowest levels are centered at about 50, 250, 600, and 1100 m above the surface. For computational expediency we degrade the horizontal resolution to 4° × 5° but retain the original vertical resolution.

Table 1. Global Atmospheric Budget of Acetone

	Singh et al. [1994][a]	*Brasseur et al.* [1998]	*Wang et al.* [1998a]	*Collins et al.* [1999]	*Singh et al.* [2000][a]	This Work (A Priori)	This Work (A Posteriori)[b]
Inventory[c], Tg						4.0	3.8
Sources[d], Tg yr^{-1}	40 (30–46)	45	60	70	56 (37–80)	78 ± 27	95 ± 15
1, Anthropogenic emissions	0.8 (0.6–1.0)	2	2	3	2 (1–3)	1.3 ± 0.7	1.1 ± 0.5
2, Biomass burning	10 (8–12)	14	14		5 (3–10)	3.4 ± 1.7[e]	4.5 ± 1.6
3 and 4, Terrestrial vegetation[f]	9 (4–18)	18	24		15 (10–20)	26 ± 20[f]	33 ± 9[f]
5, Plant decay					6 (4–8)	9 ± 9	2 ± 5
6, Ocean (phtochemical)						10 ± 10	27 ± 6
7, Isoalkanes (anthropogenic)	19 (16–23)	11	20	27	16 (11–22)[g]	20 ± 10[h]	21 ± 5
Isobutene + isopentene	1 (1–2)				1 (1–2)	0	0
8 and 9, Monoterpenes and methylbutenol[i]				40	11 (7 − 15)	9 ± 4	7 ± 3
Sinks, Tg yr^{-1}	40 – 60					78	95
Oxidation by OH	10 – 14					25[j]	27[j]
Photolysis	26 – 38					44[k]	46[k]
Dry deposition	5 – 7					9[l]	23[m]

[a] Best estimates with range in parentheses.
[b] Optimized sources from the inversion analysis of section 4. The stated errors are likely too low because of unresolved biases and correlations in the observations (see text).
[c] Troposphere only.
[d] The numbering of sources identifies the $n = 9$ elements of the state vector **x** in the inverse model analysis of section 4.
[e] Including 2.7 Tg yr^{-1} from direct emission and 0.7 Tg yr^{-1} from atmospheric oxidation of propane.
[f] The terrestrial vegetation source in this work resolves contributions from grasslands (source 3) and other terrestrial vegetation (source 4). The source from grasslands is 8 ± 8 Tg yr^{-1} (a priori) or 13 ± 7 Tg yr^{-1} (a posteriori). The source from other terrestrial vegetation is 18 ± 18 Tg yr^{-1} (a priori) or 19 ± 9 Tg yr^{-1} (a posteriori).
[g] Including 15 (10–20) Tg yr^{-1} from propane and 1 (1–2) Tg yr^{-1} from isobutane and isopentane.
[h] Including 13 Tg yr^{-1} from propane, 4.0 Tg yr^{-1} from isobutane, and 2.6 Tg yr^{-1} from isopentane.
[i] This work resolves contributions from oxidations of monotorpenes (source 8) and oxidation of methylbutenol (source 9). The source from monotorpenes is 7 ± 4 Tg yr^{-1} (a priori) or 6 ± 3 Tg yr^{-1} (a posteriori). The source from methylbutenol is 1.8 ± 1.8 Tg yr^{-1} (a priori) or 1.4 ± 1.2 Tg yr^{-1} (a posteriori).
[j] Including <1 Tg yr^{-1} in the stratosphere.
[k] Including 4 Tg yr^{-1} in the stratosphere.
[l] Deposition to land only.
[m] Including 14 Tg yr^{-1} deposited to oceans and 9 Tg yr^{-1} deposited to land.

[4] Sources of acetone to the atmosphere include direct emission as well as atmospheric oxidation of organic precursors (Table 1). Hydrocarbons with the isostructure $(CH_3)_2CH$-, monoterpenes, and methylbutenol are known atmospheric precursors of acetone [*Singh and Hanst*, 1981; *Chatfield et al.*, 1987; *Singh et al.*, 1994; *Alvarado et al.*, 1999; *Reissell et al.*, 1999; *Orlando et al.*, 2000]. Monoterpenes and methylbutenol are emitted by vegetation and have atmospheric lifetimes against oxidation of only a few hours. They do not need to be transported in the model and can instead be emitted as acetone with a scaling factor representing their acetone yield from oxidation. The C_{3-5} isoalkanes (propane, isobutane, isopentane) have atmospheric lifetimes in excess of a day against reaction with OH, their main atmospheric sink, and therefore they must be transported in the model. Higher isoalkanes as well as isoalkenes (such as 2-methyl 2-butene) also produce acetone, but emission inventories and measurements in urban air indicate that they are far less important than the C_{3-5} isoalkanes [*Middleton et al.*, 1990; *Singh and Zimmerman*, 1992], and we neglect them here.

[5] Our simulation of acetone thus includes four transported species: acetone, propane, isobutane (2-methyl-propane), and isopentane (2-methylbutane). Concentrations of these species depend linearly on their sources because the sinks are first order (chemical coupling with OH is negligible). We take advantage of this linearity by transporting acetone and isoalkanes from individual sources as separate tracers and using archived daily 3-D fields of tropospheric OH concentrations from a GEOS-CHEM simulation of tropospheric ozone-NO_x-hydrocarbon chemistry for 1994 [*Bey et al.*, 2001]. A standard test of the OH concentration computed in a global model is the lifetime of methylchloroform against tropospheric oxidation by OH [*Prinn et al.*, 1995]. The OH concentration fields from *Bey et al.* [2001] yield a methylchloroform lifetime of 5.1 years, as compared to a best estimate from observations of 5.5 years [*Spivakovsky et al.*, 2000]. We also account for oxidation of isoalkanes and acetone in the stratosphere by using monthly mean OH concentrations from a global 2-D model [*Schneider et al.*, 2000]. Additional losses of acetone from photolysis and deposition are discussed in section 2.3.

[6] Rate constants for the oxidation of isoalkanes by OH are from *Atkinson* [1997]. We use acetone yields of 0.72 mol mol^{-1} for propane, 0.93 mol mol^{-1} for isobutane, and 0.53 mol mol^{-1} for isopentane on the basis of the detailed chemical mechanism of *Madronich and Calvert* [1989] and assuming that the organic peroxy radical intermediates of hydrocarbon oxidation react exclusively with NO.

[7] We conduct a 18-month simulation from July 1993 to December 1994 initialized with concentration fields from *Bey et al.* [2001]. The first 6 months are used to achieve proper initialization, and we focus our analysis on the 12-month simulation for 1994.

2.2. Sources of Acetone

[8] Here we construct a set of best a priori estimates of global acetone sources for use in the model. Depending on the quality of

Table 2. Atmospheric Observations of Acetone

	Period	References	Number of Observation Elements[a]
Surface sites			
Nine European sites (see Figure 7)	1992–1995	*Solberg et al.* [1996]	84
Dorset and Egbert, Ontario	Aug. 1998	*Shepson et al.* [1991]	1[b]
Kinterbish, Alabama	June–July 1990	*Goldan et al.* [1995]	2
Mettler, Georgia	July–Aug. 1991, June 1992	*Lee et al.* [1995]	3
Youth, Inc., Tennessee	June1995	*Riemer et al.* [1998]	1
Blodgett Forest, California	July–Aug. 1997, 1998, 1999	*Goldstein and Schade* [2000]	0[c]
Ahmeek, Michigan	Jan. 1999	*Couch et al.* [2000]	1
Alert, Nunavut	April 1986, 1992, 1994	*Bottenheim et al.* [1990] *Yokouchi et al.* [1994] *Shepson at al.* [1996]	0[d]
Aircraft missions[e]			
SONEX, North Atlantic regions 1–2	Oct.–Nov. 1997	*Singh et al.* [2000]	5
ABLE-3B, E Canada region 3	July–Aug. 1990	*Singh et al.* [1994]	2
PEM-West B, NW Pacific (PWB) regions 4–7	Feb.–March 1994	*Singh et al.* [1995]	11
TRACE-A, South Atlantic (TA) regions 8–13	Sept.–Oct. 1992	*Jacob et al.* [1996]	17
PEM-Tropics B, tropical Pacific (PEMTB) regions 14–18	March–April 1999	*Singh et al.* [2001]	15

[a] Adding up to the $m = 142$ elements of the observation vector **y** in the inversion model analysis of section 4. For surface sites the monthly mean concentrations represent individual observation elements. For aircraft missions the mean concentrations at 0–4, 4–8, and 8–12 km altitude for each of the regions of Figure 4 represent individual observation elements.

[b] Observations from the two sites have been combined because the sites are nearby and values are similar.

[c] The observations at the Blodgett Forest mountain site are not used in the inversion analysis because of concern over the influence of local orographic circulations, but the acetone source apportionment derived for that site by *Goldstein and Schade* [2000] is compared to model results in section 5.

[d] The observations at Alert are not used in the inversion analysis because of concern over their quality but are used for comparison to model results (Figure 8).

[e] Region numbers refer to Figure 4.

the estimates, we assign relative errors of either 50% or 100% (Table 1). Atmospheric observations of acetone will be used in sections 4 and 5 to improve these estimates and to reduce the errors.

2.2.1. Anthropogenic emission. [9] Anthropogenic emission of acetone includes contributions from solvent use and automobiles [*Singh et al.*, 1994]. We use the EDGAR V2.0 anthropogenic emission inventory for alkanones in 1990 with $1° \times 1°$ horizontal resolution and no seasonal variation [*Olivier et al.*, 1994] and assume that acetone accounts for 50% of total alkanone emissions. The resulting a priori global source of acetone is 1.3 ± 0.7 Tg yr^{-1}.

2.2.2. Biomass burning. [10] A review by *Andreae and Merlet* [2001] gives acetone/CO molar emission ratios of 0.2–0.3% depending on vegetation type. We apply these ratios to a climatological biomass burning emission inventory for CO with $1° \times 1°$ spatial resolution and monthly temporal resolution based on satellite data [*Duncan et al.*, 2001]. The global CO emission in that inventory is 420 Tg yr^{-1} from which we infer an a priori acetone emission from biomass burning of 2.7 ± 1.4 Tg yr^{-1}. Emission of acetone from biofuels is negligible [*Andreae and Merlet*, 2001].

2.2.3. Terrestrial vegetation. [11] Acetone is emitted from vegetation as a by-product of plant metabolism [*Fall*, 1999]. *Kirstine et al.* [1998] measured acetone emission fluxes from grass canopies and found a light and temperature dependence similar to that of isoprene, with large variability between grass types and high emissions from grasses that do not emit isoprene. By global extrapolation they estimated a direct acetone source from grasslands of 8 Tg yr^{-1} which we adopt as a priori (8 ± 8 Tg yr^{-1}). We distribute this source globally over all grasslands in the *Olson* [1992] land-type database ($0.5° \times 0.5°$ spatial resolution), using the isoprene emission model of *Guenther et al.* [1995] to specify light and temperature dependences.

[12] Acetone concentration measurements at rural sites in the United States in summer show a strong correlation with methanol with slope of 0.21–0.27 mol mol^{-1} [*Goldan et al.*, 1995; *Riemer et al.*, 1998; *Schade and Goldstein*, 2001]. Vegetation is thought to be the main source of atmospheric methanol, with a global emission in the range 50–100 Tg yr^{-1} [*Singh et al.*, 2000]. Scaling by 0.21–0.27 mol mol^{-1} implies a global vegetation source of acetone in the range 20–50 Tg yr^{-1}, or a best estimate of 35 Tg yr^{-1}. Subtracting the contributions from grasslands (8 Tg yr^{-1}) and from atmospheric oxidation of monoterpenes and methylbutenol (9 Tg yr^{-1}, given below), which we assume contribute to the observed acetone/methanol correlations, leaves a best a priori estimate for a residual "nongrassland" direct vegetative emission of 18 ± 18 Tg yr^{-1}. We distribute this source in the model following isoprene emissions, as suggested by the data of *Goldan et al.* [1995] and *Riemer et al.* [1998].

2.2.4. Plant decay. [13] *Warneke et al.* [1999] reported the abiotic emission of acetone from decaying plant matter with an estimated emission factor of $\sim 1 \times 10^{-4}$ g per g of C oxidized. Field measurements by *Schade and Goldstein* [2001] indicate a soil emission of acetone that could be either abiotic or microbial in origin. We apply the emission factor of *Warneke et al.* [1999] to a global inventory of monthly mean heterotrophic respiration rates with $1° \times 1°$ resolution from the CASA 2 Biosphere Model [*Potter et al.*, 1993]. Global respiration rates in that inventory are 90 Pg C yr^{-1}, and the resulting a priori acetone source is 9 ± 9 Tg yr^{-1}.

2.2.5. Atmospheric oxidation of isoalkanes. [14] Atmospheric oxidation of C_3–C_5 isoalkanes is a major source of acetone [*Singh et al.*, 1994], but global emission rates of isoalkanes are poorly known. Sources include leakage of natural gas (propane), leakage of liquified petroleum gas (propane, isobutane), and automobile fuel evaporation (isobutane, isopentane) [*Middleton et al.*, 1990; *Blake and Rowland*, 1995]. The most detailed global emission inventory is EDGAR V2.0

[*Olivier et al.*, 1994], which resolves propane, total butanes, and total pentanes emissions. Measurements in urban air show that isobutane accounts for ~30% of total butanes emissions and isopentane accounts for ~65% of total pentanes emissions [*Goldan et al.*, 2000; *Saito et al.*, 2000]. Applying these fractions to the EDGAR inventory, we obtain global emission totals of 5.5 Tg C yr^{-1} for propane, 3.5 Tg C yr^{-1} for isobutane, and 6.1 Tg C yr^{-1} for isopentane.

[15] We find, however, that when implemented in our model, the EDGAR inventory underestimates considerably the observed atmospheric concentrations of propane and isobutane over Europe, over the United States, and downwind of Asia, as illustrated in Figures 1 and 2. EDGAR emissions of propane are highly concentrated in the Middle East and are very low elsewhere; this distribution appears to be seriously in error. Instead, we adopt the global paraffin emission inventory of *Piccot et al.* [1992], updated for 1994 as described by *Bey et al.* [2001] and speciated on the basis of U.S. data as described by *Wang et al.* [1998a] (total paraffins in this speciation include 15% propane, 5% isobutane, and 7% isopentane on a carbon basis). Concentrations simulated with that inventory are still too low downwind of Asia and in the Southern Hemisphere, which may be expected since the inventory uses hydrocarbon emission factors based on data from the United States where emissions are strongly controlled. In order to better match the atmospheric observations we double the *Piccot et al.* [1992] emission estimates for all countries outside Europe and North America. The resulting global anthropogenic source of paraffins for 1994 is 73 Tg C yr^{-1} from which we deduce isoalkane emissions of 11 Tg C yr^{-1} propane, 3.6 Tg C yr^{-1} isobutane, and 5.0 Tg C yr^{-1} isopentane.

[16] Biomass burning is only a small source of isoalkanes. Measured propane/CO molar emission ratios for different vegetation types are in the 0.1–0.2% range [*Andreae and Merlet*, 2001]. With a global CO source of 420 Tg yr^{-1} from biomass burning, we estimate a corresponding propane source of 0.64 Tg C yr^{-1}. Biomass burning emissions of isobutane and isopentane are only a few percent of propane emissions [*Blake et al.*, 1994; *Ferek et al.*, 1998] and are neglected.

[17] Biogenic sources of C_3–C_5 isoalkanes appear to be negligibly small. Measured concentration ratios at urban and rural North American sites [*Jobson et al.*, 1994; *Goldstein et al.*, 1995; *Goldan et al.*, 2000] and over the ocean [*Saito et al.*, 2000] are consistent with anthropogenic emission ratios; there is no evidence for a significant background maintained by biogenic sources. Seawater concentration measurements compiled by *Plass-Dulmer et al.* [1995] indicate global oceanic sources of 0.1 Tg yr^{-1} for propane and 0.06 Tg yr^{-1} for butanes. These sources would contribute <1 pptv in the marine boundary layer and are neglected.

[18] We compared the isoalkane concentrations simulated by the model to a large number of year-round observations at ground-based sites [*Shepson et al.*, 1991; *Goldstein et al.*, 1995; *Solberg et al.*, 1996; *Clarkson et al.*, 1997] and vertical profiles from aircraft missions [*Blake et al.*, 1992, 1994, 1996, 1997, 1999, 2001]. Representative results for ground-based sites are shown in Figure 1 with data from Rucava (Lithuania), Harvard Forest (Massachusetts), and a composite of Baring Head (New Zealand)

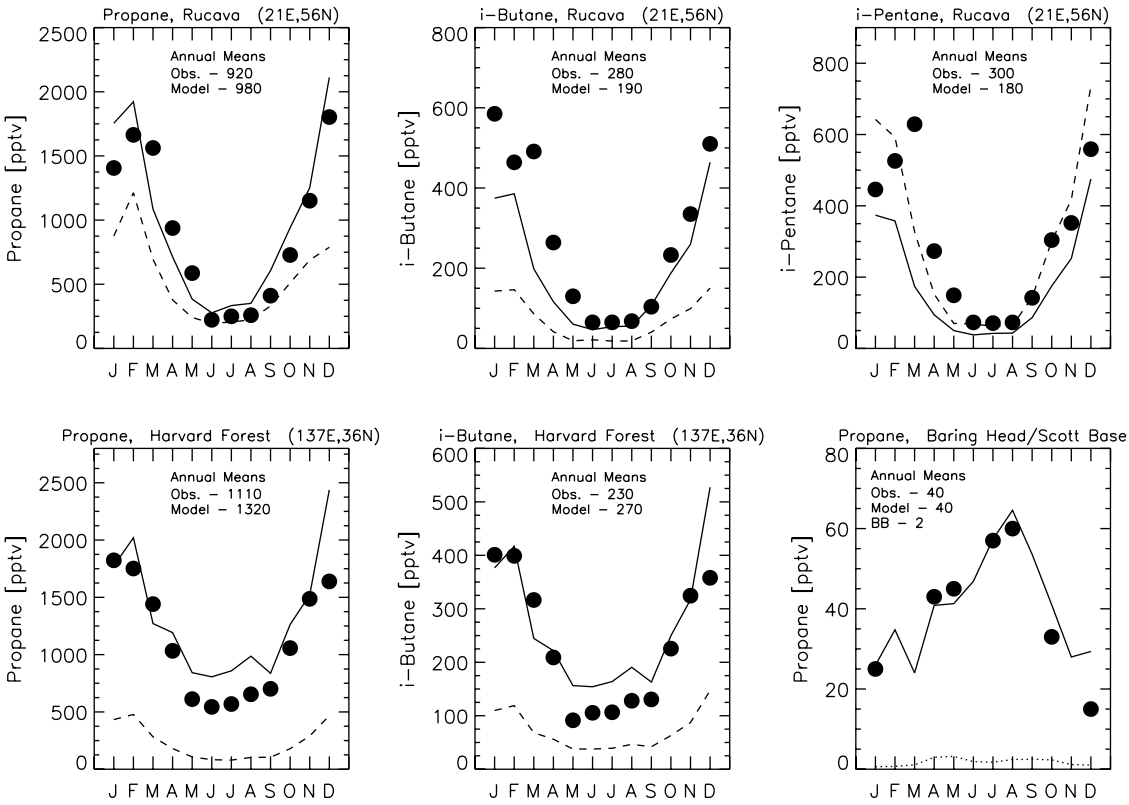

Figure 1. Seasonal variation of monthly mean propane, isobutane, and isopentane concentrations at nonurban surface sites. Values are monthly means. Observations (symbols) are from *Solberg et al.* [1996] at Rucava (Lithuania), *Goldstein et al.* [1995] at Harvard Forest (United States), and *Clarkson et al.* [1997] at Baring Head (New Zealand) and Scott Base (Antarctica). The data at Baring Head and Scott Base are similar and have been combined following *Clarkson et al.* [1997]. Model results are shown as solid lines for the standard simulation and as dashed lines for the simulation using the EDGAR V2.0 emission inventory. The dotted line in the Baring Head/Scott Base plot shows the contribution from biomass burning to simulated propane concentrations. Annual mean concentrations are given for the observations and for the standard model simulation.

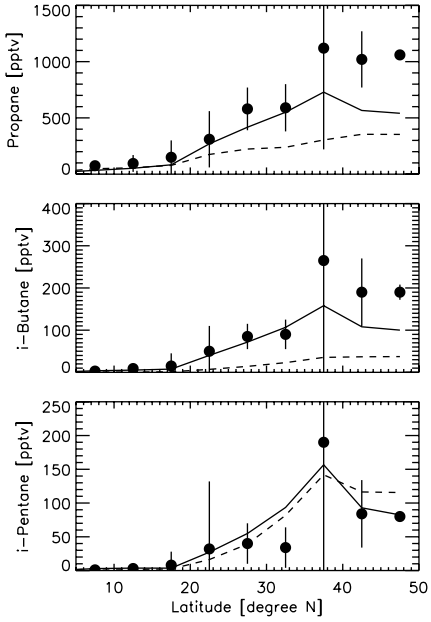

Figure 2. Latitudinal distributions of propane, isobutane, and isopentane concentrations at 0–6 km altitude over the western Pacific in February–March 1994. Mean observations from the PEM-West B aircraft mission [*Blake et al.*, 1997] are shown as symbols, with vertical bars showing the corresponding standard deviations. Model results are shown as solid lines (standard simulation) and dashed lines (simulation with EDGAR V2.0 emissions).

and Scott Base (Antarctic Coast). Observations at northern mid-latitudes sites show a strong seasonal cycle reflecting that of OH [*Goldstein et al.*, 1995]. The simulated annual means and relative seasonal amplitudes of propane concentrations for the ensemble of sites that we examined in Europe and North America are on average within 10% of observations, supporting the propane emission estimates (the successful simulation of the relative seasonal amplitude constrains independently the loss rate constant from oxidation by OH). Annual mean concentrations of isobutane and isopentane simulated by the model are too low on average by 20% and 30%, respectively, and the seasonal variations are higher than observed. *Solberg et al*. (1986) previously noted the relatively weak seasonal cycle in isobutane and isopentane observations at the European sites and attributed it to a summer maximum in emissions from fuel evaporation.

[19] Simulated propane concentrations at Baring Head and Scott Base match well the *Clarkson et al.* [1997] observations. *Clarkson et al.* [1997] argued that propane at these two sites is mostly from biomass burning, but the emission factor that they used to reach this conclusion is an order of magnitude higher than the best estimate of *Andreae and Merlet* [2001] which is supported by extensive data. Biomass burning in our simulation makes a negligibly small contribution to propane at Baring Head and Scott Base (1 pptv on an annual mean basis). The main source is anthropogenic and includes contributions from emissions in both hemispheres. The observed late winter maximum, which the model captures well, is mainly determined by the seasonal cycle of OH concentrations.

[20] To evaluate the isoalkane emission estimates for eastern Asia, we examined data from the Pacific Exploratory Mission (PEM)-West B aircraft mission over the western Pacific in February–March 1994, which sampled a strong Asian outflow north of 20°N and below 6 km altitude [*Blake et al.*, 1999]. Results in Figure 2 show no evident model bias in the 20°–40°N latitude range, which is the core of the Asian outflow. Concentrations of propane and isobutane north of 40°N are underestimated, but the observations there are less representative of Asian outflow and could reflect in part the seasonal accumulation of hydrocarbons at high latitudes.

[21] Additional comparisons of model results to observed vertical concentration profiles are shown in Figure 3 for selected regions from Figure 4 (only for propane; observations for isobutane and isopentane are frequently below the detection limit). The model has some success in reproducing the observed latitudinal and vertical gradients of propane concentrations, and there is no general bias that would imply a bias in the model emissions. During the TRACE-A flights off the western African coast the lower troposphere was heavily affected by biomass burning outflow [*Mauzerall et al.*, 1998], but only a small enhancement of propane was observed (Figure 3), further arguing against a major biomass burning source of propane in the Southern Hemisphere.

[22] Our estimate of the global source of propane is 70% higher than the value of 6.9 Tg C yr^{-1} estimated by *Gupta et al.* [1998] by fitting surface air observations along the Pacific Rim with a global 2-D (altitude-latitude) model. The observations used by *Gupta et al.* [1998] are from relatively remote sites, and interpreting them as zonal means for comparison to the 2-D model could have intro-

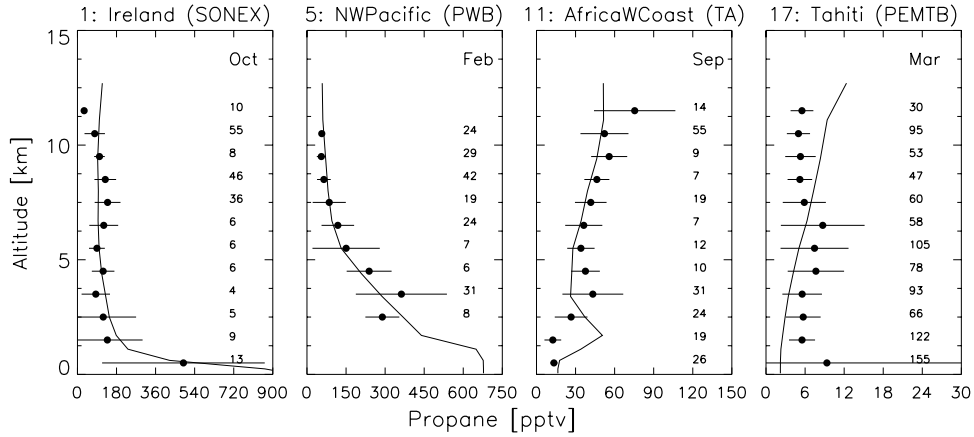

Figure 3. Vertical profiles of propane concentrations averaged over coherent geographical regions (the numbering of regions corresponds to Figure 4). Observations are from the aircraft missions of Table 2. Symbols are mean observed values (with standard deviations and numbers of observations indicated). Lines are monthly mean model values.

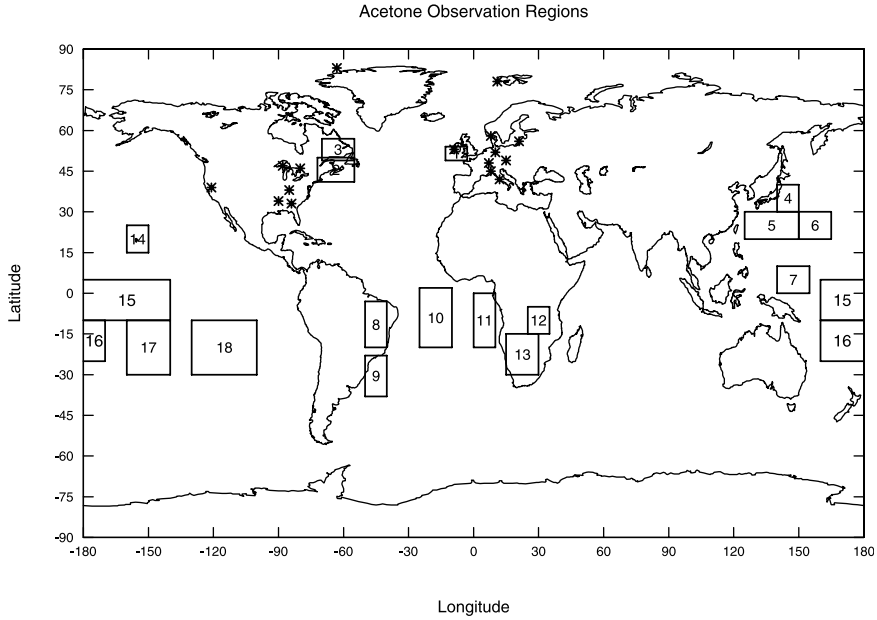

Figure 4. Acetone measurement sites (symbols) and coherent regions used to average aircraft observations for purposes of model evaluation and inverse model analysis (Table 2). The regions are the same as those used by *Bey et al.* [2001] for general GEOS-CHEM model evaluation.

duced some low bias in the emission estimate. *Phadnis and Carmichael* [2000] used a mesoscale model for east Asia with a regional propane source of 1.3 Tg C yr^{-1} (as compared to 2.3 Tg C yr^{-1} here for the same region) to simulate 1987 observations of propane over China and Japan. It seems from their comparisons to observations that they could accommodate an increase in the regional propane source to our level, and one also has to account for growth in Asian emissions from 1987 to 1994.

[23] In summary, we consider the propane emissions used in the model to have no apparent bias; the isobutane and isopentane emissions are not as well constrained and could be too low. Using the acetone yields from section 2.1, we estimate a priori sources of acetone of 14 Tg yr^{-1} from propane (including 0.7 Tg yr^{-1} from biomass burning), 4.0 Tg yr^{-1} from isobutane, and 2.6 Tg yr^{-1} from isopentane, for a total acetone source of 21 ± 10 Tg yr^{-1} from atmospheric oxidation of isoalkanes.

2.2.6. Atmospheric oxidation of monoterpenes. [24] *Reissell et al.* [1999] measured acetone yields for the oxidation of a suite of monoterpenes by OH and ozone in the presence of NO. By applying these yields to a speciated monoterpene emission inventory for North America [*Guenther et al.*, 2000] and assuming typical OH and ozone concentrations of 2×10^6 and 1×10^{12} molecules cm^{-3}, respectively, we obtain a weighted average molar yield of 0.12 for production of acetone from oxidation of monoterpenes. We extrapolate this yield to the global unspeciated emission inventory for monoterpenes from *Guenther et al.* [1995]. Monoterpene emissions in that inventory are a function of local vegetation type, leaf area index, and temperature. We use the land-type map from *Olson* [1992], calculate local leaf area indices with the algorithm of *Guenther et al.* [1995] as modified by *Wang et al.* [1998a], and apply local surface air temperatures from the GEOS meteorological data. The resulting global monoterpene emission rate is 120 Tg C yr^{-1}, which yields an a priori acetone source of 7 ± 4 Tg yr^{-1}.

2.2.7. Atmospheric oxidation of methylbutenol. [25] Methylbutenol is emitted by vegetation, and its main atmospheric sink is reaction with OH. Laboratory measurements by *Alvarado et al.* [1999] indicate a 0.58 mol mol^{-1} yield of acetone from this reaction in the presence of NO. Large emissions of methylbutenol have been observed from pine forests in western North America but not elsewhere in the world; the emission flux depends on light and temperature similarly to isoprene [*Harley et al.*, 1998; *Baker et al.*, 1999]. *Guenther et al.* [2000] give a methylbutenol emission inventory of 3.2 Tg C yr^{-1} for North America, corresponding to an a priori acetone source of 1.8 ± 1.8 Tg yr^{-1}. We distribute this source over pine forest land types following the light and temperature dependence of isoprene emission, and assume no source outside North America.

2.3. Sinks of Acetone

[26] The model includes acetone losses from oxidation by OH, photolysis, and deposition to land and ocean. Deposition to the ocean will be discussed in section 2.4. The rate constant for oxidation of acetone by OH is $k = 8.8 \times 10^{-12}\exp[-1320/T] + 1.7 \times 10^{-14}\exp[423/T]$ cm^3 $molecule^{-1}$ s^{-1} [*Wollenhaupt et al.*, 2000]. Photolysis is computed using temperature-dependent absorption cross sections and pressure-dependent quantum yields from *Gierczak et al.* [1998] and local UV actinic fluxes from the Fast-J radiative transfer code [*Wild et al.*, 2000; *Cameron-Smith*, 2000] applied within GEOS-CHEM [*Bey et al.*, 2001].

[27] Microbial activity in the terrestrial biosphere is both a source and a sink for acetone. Diurnal cycles of atmospheric acetone concentrations at eastern North American sites in summer show typically a 20% decrease from sunset to sunrise [*Shepson et al.*, 1991; *Goldan et al.*, 1995; *Lee et al.*, 1995] which could reflect microbial uptake. On the other hand, acetone flux measurements by *Schade and Goldstein* [2001] at a California mountain site indicate a weak net emission from the soil at night. We include in the model a dry deposition velocity of 0.1 cm s^{-1} for acetone to ice-free land, designed to yield a 20% decrease in concentrations from sunset to sunrise for a 100-m-deep nighttime mixed layer in the absence of compensating emission. The resulting global sink in the model is comparable in magnitude to the soil source from plant decay (Table 1) and the uncertainties on the two cannot be separated.

[28] We assume no deposition to ice or snow. Recent observations in Arctic spring indicate that the snow surface, in fact, provides a daytime source and a nighttime sink for acetone, the

two largely cancelling each other over the diurnal cycle [*Grannas*, 2002; *Guimbaud et al.*, 2002].

2.4. Exchange With the Ocean

[29] The standard approach for calculating the sea-to-air flux F of a gas is with the two-film model of *Liss and Slater* [1974]:

$$F = K_G(HC_L - C_G). \quad (1)$$

Here C_G and C_L are the concentrations in the bulk atmospheric and oceanic phases, H is the dimensionless Henry's law constant defined as the ratio of the concentration in air to that in seawater (for acetone $H_{298} = 1.4 \times 10^{-3}$ at 298 K, $\Delta H/R = 5500$ K [*Zhou and Mopper*, 1990]), and K_G is a transfer velocity:

$$K_G = \left(\frac{H}{k_L} + \frac{1}{k_G}\right)^{-1}, \quad (2)$$

where k_L and k_G are conductances for mass transfer in the liquid and gas phase for which we adopt the parameterizations of *Nightingale et al.* [2000] and *Liss* [1973], respectively, as a function of wind speed.

[30] For typical wind speeds, K_G is in the range 0.1–1 cm s^{-1}, sufficiently high that uptake by the ocean must be considered as a major sink for acetone unless it is reversible. The solubility of acetone is such that diffusion in either the gas phase or the liquid phase may limit mass transfer depending on wind speed (that is, the terms H/k_L and $1/k_G$ in equation (2) are of similar magnitude).

[31] Microbial and photochemical activity in the ocean may provide either a net sink or a net source of acetone. Microbial activity is usually a net sink [*Kieber et al.*, 1990], while photochemical degradation of dissolved organic matter (DOM) by UV-B radiation (290–320 nm) is a source [*Blough*, 1997; *Zhou and Mopper*, 1997]. To our knowledge, the only seawater measurements of acetone in the literature are those of *Zhou and Mopper* [1997], who found concentrations of 3.0 ± 0.2 nM in subsurface bulk water and 55 ± 2 nM in the surface organic microlayer in samples from the North Atlantic. Atmospheric boundary layer concentrations in the region are ~0.4 ppbv [*Zhou and Mopper*, 1993], corresponding to an equilibrium seawater concentration of 12 nM at 298 K. *Zhou and Mopper* [1997] attributed the high concentrations in the surface microlayer to enrichment in DOM and exposure to strong UV radiation.

[32] Additional support for an oceanic source of acetone is offered by the PEM-Tropics B aircraft measurements of *Singh et al.* [2001] over the South Pacific in March–April, which indicate 0.4 ppbv acetone with little variability. As pointed out by Singh et al., such high concentrations and low variability cannot be reconciled with long-range transport of acetone from continental sources and suggest instead a source of acetone from the ocean or from the marine atmosphere.

[33] On the basis of the above information we parameterize the sea-to-air flux of acetone in the model as

$$F = K_G\left[H\alpha J_{O(1D)} - (1-R)C_G\right], \quad (3)$$

where $J_{O(1D)}$ is the 24-Bhour average photolysis frequency of ozone to $O(^1D)$ in surface air, which provides a measure of the UV-B flux, α is a constant coefficient, and R is the saturation ratio of acetone in the subsurface ocean relative to the atmosphere. The first term $P = K_G H\alpha J_{O(1D)}$ in equation (3) represents the photochemical source. The second term $L = (1 - R)K_G C_G$ represents microbial oceanic uptake, where the value of R may range from 1 (equilibrium between the atmosphere and the subsurface seawater) to 0 (fast consumption in seawater). In the lower limit of no ocean uptake ($R = 1$, $L = 0$) we find that a global photochemical source $P = 10$ Tg yr^{-1} (corresponding to $\alpha = 1.5 \times 10^{-8}$ kg s cm^{-3}) is needed to roughly match the *Singh et al.* [2001] observations over the South Pacific. In the upper limit of mass transfer limited ocean uptake ($R = 0$) we would need a source of about $P = 60$ Tg yr^{-1} to balance the corresponding sink

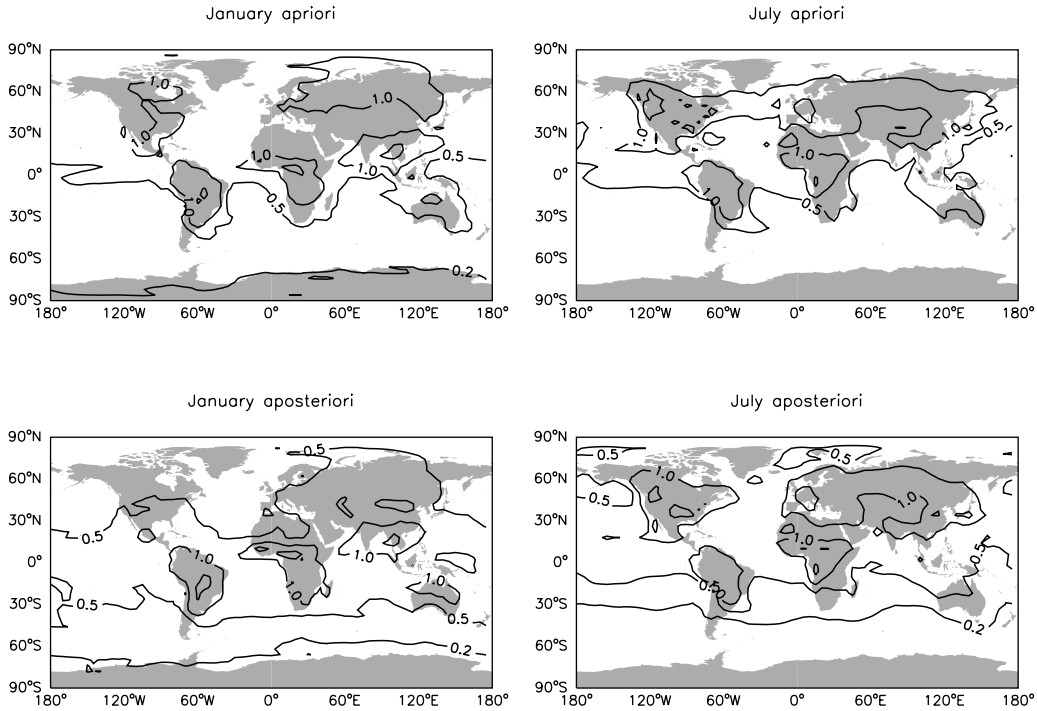

Figure 5. Simulated acetone concentrations (ppbv) in surface air for January and July using (top) the a priori sources and no ocean sink and (bottom) the a posteriori sources and an ocean sink (saturation ratio $R = 0.85$). Values are monthly means. Contours are 0.1-0.2-0.5-1-2-5 ppbv.

L = 50 Tg yr^{-1}. We choose the lower limit P = 10 ± 10 Tg yr^{-1} with no ocean uptake as a priori because it minimizes the role of the ocean in the atmospheric budget of acetone. Improved values of P and R for matching the observed atmospheric concentrations of acetone will be derived in section 4.

3. A Priori Budget and Simulated Distribution of Acetone

[34] Table 1 summarizes our global a priori budget of acetone and compares it to previous estimates. Our global source is larger, in part because of our consideration of an oceanic source. Our biomass burning source is lower and is probably more reliable in view of current knowledge of emission factors [*Andreae and Merlet*, 2001; M. O. Andreae, personal communication, 2001]. Our source from terrestrial vegetation is higher but poorly constrained. Our source from abiotic plant decay is higher than that of *Singh et al.* [2000] and is absent in the other estimates of Table 1. Our estimate of the total secondary source of acetone from atmospheric oxidation of organic compounds is close to that of *Singh et al.* [2000] but much higher than the older estimates which did not include production from monoterpenes or methylbutenol. *Collins et al.* [1999] have an anomalously large secondary source from monoterpenes which probably also serves in their model as a parameterization of direct emission from vegetation.

[35] Our global 3-D model simulation with a priori sources yields a mean tropospheric lifetime for acetone of 20 days. Photolysis and oxidation by OH in the troposphere contribute 51% and 32% of the atmospheric sink of acetone, respectively, dry deposition to land contributes 12%, and photolysis in the stratosphere contributes 3% (Table 1). Additional loss to the ocean will be considered below and reduces the tropospheric lifetime of acetone to 15 days. *Singh et al.* [1994] previously obtained a similar acetone lifetime from a global 3-D model and partitioned the sink as 64% from photolysis, 24% from oxidation by OH, and 12% from deposition, consistent with our values.

[36] Figure 5 (top) shows the simulated concentrations of acetone in surface air for January and July using the a priori sources. Concentrations over continents are typically 0.5–2 ppbv and tend to be higher in summer than in winter. The relative contributions from different sources are highly variable with region and season. Over the tropical continents the principal sources are from terrestrial vegetation and plant decay, with an additional seasonal contribution from biomass burning. Over the northern midlatitude continents the dominant sources in winter are from oxidation of propane, anthropogenic emission, and plant decay; terrestrial vegetation becomes the dominant source in summer. The high values over northwest North America in summer are due to oxidation of methylbutenol. Further discussion of the relative contributions from different sources to acetone concentrations will be presented in section 5 in the context of comparisons to observations.

[37] Simulated acetone concentrations in the marine boundary layer are typically 0.5–1 ppbv in the Northern Hemisphere and 0.3–0.5 ppbv in the Southern Hemisphere. The higher values in the north are due to continental influence. Oceanic emission is a major source in the south. Concentrations drop to below 0.2 ppbv over Antarctica in summer, reflecting the remoteness of sources and the seasonal photochemical sink.

[38] Simulated acetone concentrations at higher altitudes show similar geographic patterns as at the surface but with less zonal structure. Figure 6 shows the simulated zonal mean concentrations as a function of altitude and latitude for January and July. Concentrations generally decrease with altitude. The vertical gradients are least in polar winter (due to the lack of sinks) and in the tropics (because of strong vertical mixing). The sources contribu-

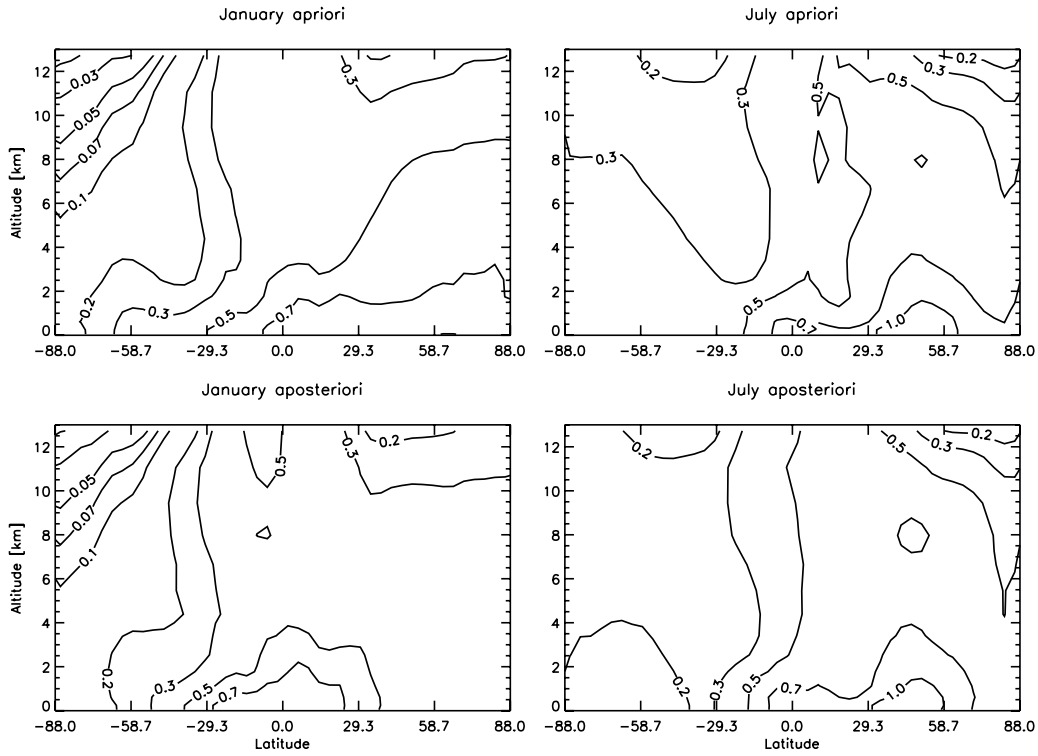

Figure 6. Simulated zonal mean acetone concentrations (ppbv) for January and July using (top) the a priori sources and no ocean sink and (bottom) the a posteriori sources and an ocean sink (saturation ratio R = 0.85). Values are monthly means.

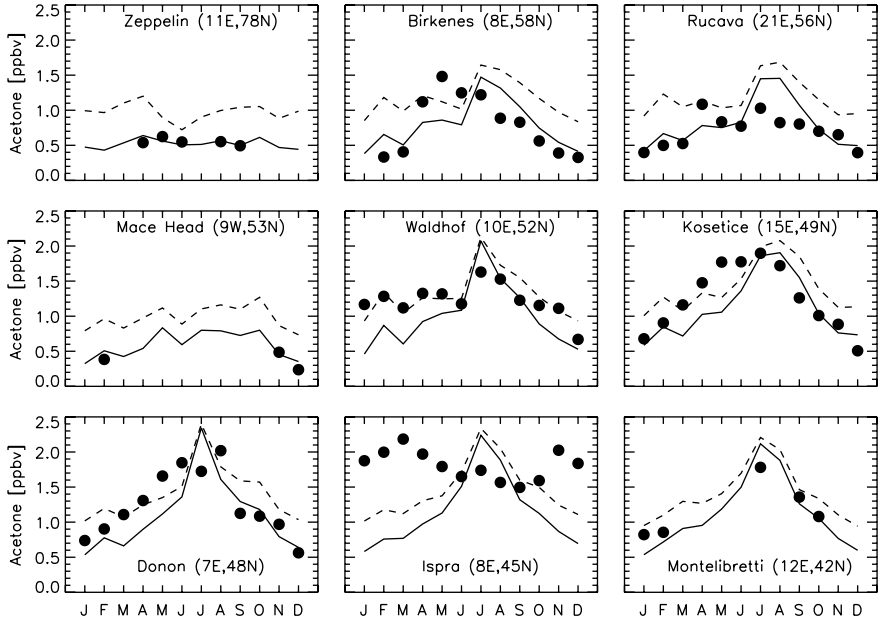

Figure 7. Seasonal variation of acetone concentrations at sites in Europe. Values are monthly means. Observations [*Solberg et al.*, 1996] are shown as symbols. The dashed line shows model results with a priori sources and no ocean sink. The solid line shows model results with a posteriori sources and an ocean sink (saturation ratio $R = 0.85$).

ting to acetone in the tropopause region, which is of particular photochemical interest, will be examined in section 6.

4. Inverse Model Analysis

[39] Simulated acetone concentrations using the forward model with a priori sources will be compared to observations in section 5. The observations contain complex information on sources, and we use an inverse model analysis to determine how this information may be used to improve the a priori estimates. We follow the notation of *Rodgers* [2000]. Let $\mathbf{y}$ be the observation vector of dimension m representing the ensemble of atmospheric measurements, and let $\mathbf{x}$ be the state vector of dimension $n = 9$ representing the global source terms numbered in Table 1 that we wish to optimize. As pointed out in section 2.1, the relationship between $\mathbf{y}$ and $\mathbf{x}$ is linear and can be obtained from the forward model:

$$\mathbf{y} = \mathbf{K}\mathbf{x} + \boldsymbol{\epsilon}. \tag{4}$$

Here $\mathbf{K}$ is a $m \times n$ Jacobian matrix with terms $k_{ij} = \partial y_i / \partial x_j$ calculated from the forward model, and $\boldsymbol{\epsilon}$ is an "observational"

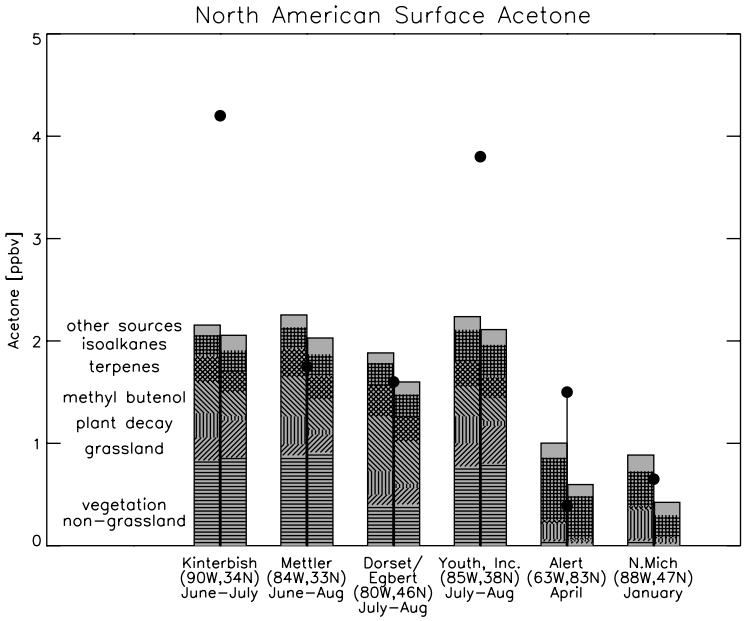

Figure 8. Concentrations of acetone at sites in North America (Table 2). Observations are shown as symbols, and model results are shown as bars (left, a priori; right, a posteriori) with contributions from individual sources presented in an additive manner. Observations for Alert are given as a range of values.

error vector with covariance matrix $\mathbf{S}_\epsilon = E\{\epsilon\epsilon^T\}$, where E is the expected value operator. We start from our a priori estimate $\mathbf{x}_a$ for the state vector (Table 1) with an error covariance matrix $\mathbf{S_a} = E\{(\mathbf{x} - \mathbf{x_a})(\mathbf{x} - \mathbf{x_a})^T\}$ whose diagonal terms are the squares of the error estimates in Table 1 (off-diagonal terms are assumed to be zero). Least squares minimization of the error in fitting the forward model to the observations leads to an optimized a posteriori value $\hat{\mathbf{x}}$ for the state vector [*Rodgers*, 2000]:

$$\hat{\mathbf{x}} = \mathbf{x_a} + \mathbf{S_a}\mathbf{K}^T\left(\mathbf{K}\mathbf{S_a}\mathbf{K}^T + \mathbf{S}_\epsilon\right)^{-1}(\mathbf{y} - \mathbf{K}\mathbf{x_a}) \quad (5)$$

with error covariance matrix $\hat{\mathbf{S}}$

$$\hat{\mathbf{S}} = \left(\mathbf{K}^T\mathbf{S}_\epsilon^{-1}\mathbf{K} + \mathbf{S_a}^{-1}\right)^{-1}. \quad (6)$$

Table 2 lists the ensemble of atmospheric measurements of acetone used for the inverse analysis. The measurements are from nonurban surface sites (Figures 7 and 8) and aircraft missions (Figure 9). From these measurements we construct an observation vector $\mathbf{y}$ with $m = 142$ elements, as detailed in Table 2. The components of $\mathbf{y}$ include monthly mean concentrations from surface sites, plus aircraft observations averaged over the 18 coherent regions of Figure 4 and then further averaged vertically over 0–4 km, 4–8 km, and 8–12 km altitude bands. The aircraft observation elements are taken to be representative of mean conditions for the month and region of observation. Most measurements are not for 1994 (the meteorological year used in the simulation); the associated error should be relatively small and we include it in the observational error vector ϵ.

[40] The error vector ϵ includes contributions from (1) measurement error, for which some information is available from intercomparisons [*Apel et al.*, 1998; *Wohlfrom et al.*, 1999]; (2) representativeness error from mismatch in time and space between the model and observations (due, for example, to interannual variability or to the assumption that aircraft observations are representative of regional and monthly means); (3) errors in the geographical and temporal distribution of the acetone sources (which we do not try to optimize); and (4) other errors in the forward model (due to incorrect representation of atmospheric transport and acetone sinks). We estimate that the ensemble of these four factors results in an overall 50% error on the individual elements of $\mathbf{y}$, and we further assume that the errors are uncorrelated. The error covariance matrix $\mathbf{S}_\epsilon$ thus has $0.25y_i^2$ as diagonal terms and zero as off-diagonal terms.

[41] We solve for $\hat{\mathbf{x}}$ and $\hat{\mathbf{S}}$ by sequential updating [*Rodgers*, 2000] in which the observation vector $\mathbf{y}$ is split into small subvectors representing observations for a given region or season. Sequential application of equations (5) and (6) to the ensemble of subvectors leads to the final solution (the a posteriori values $\hat{\mathbf{x}}$ and $\hat{\mathbf{S}}$ obtained from a given subvector are taken as a priori values $\mathbf{x_a}$ and $\mathbf{S_a}$ for the next subvector). The final solution is not affected by the size of the subvectors nor by the order in which they are applied.

[42] Acetone sinks are not included in the state vector. Loss frequencies from photolysis and reaction with OH are relatively well constrained. Deposition to land is strongly coupled to the

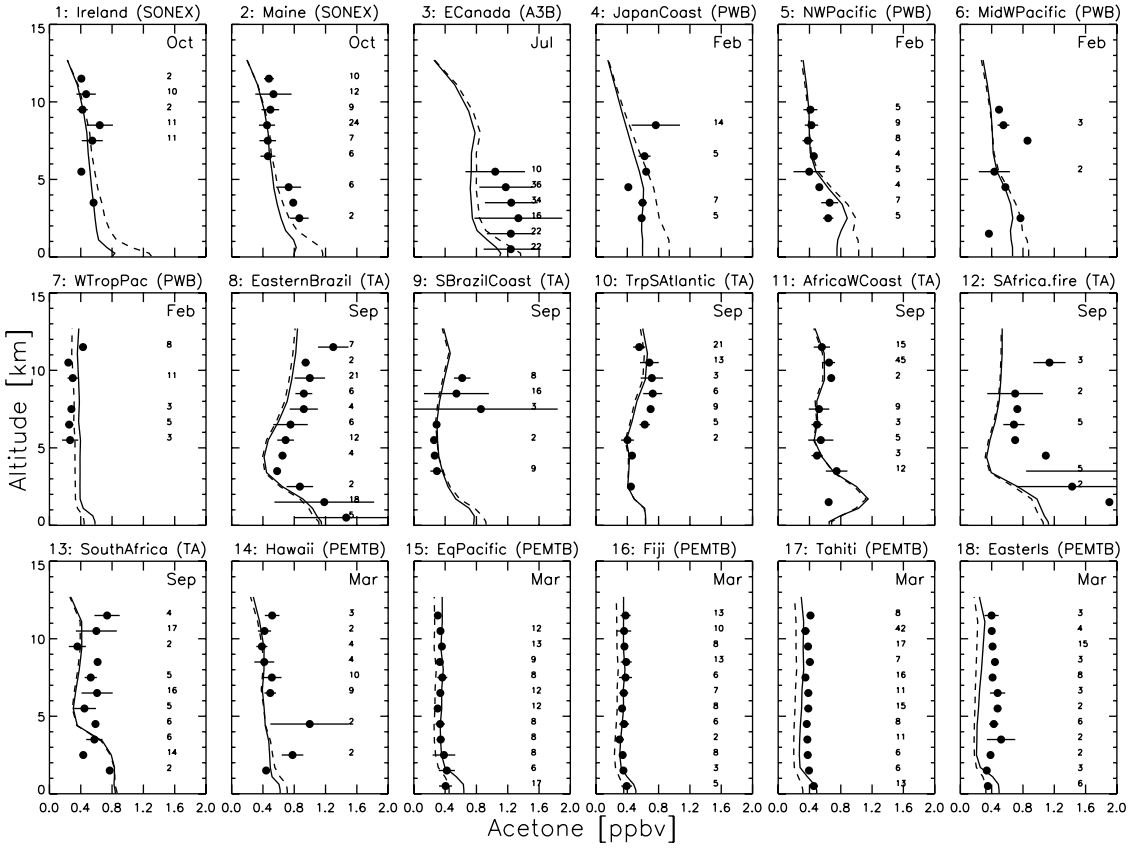

Figure 9. Comparison of simulated and observed vertical profiles of acetone concentrations. Observations are from the aircraft missions of Table 2 and are averaged over the regions in Figure 4. A3B stands for ABLE-3B, PWB for PEM-West B, TA for TRACE-A, and PEMTB for PEM-Tropics B. Symbols are mean observed values (with standard deviations and numbers of observations indicated). The dashed line shows model results with a priori sources and no ocean sink. The solid line shows model results with a posteriori sources and an ocean sink (saturation ratio $R = 0.85$). Model values are monthly means.

plant decay source, so that optimizing the latter effectively optimizes the former. Uptake by the ocean (as defined by the ocean saturation ratio R) has a nonlinear effect on the acetone concentration field, and its inclusion in the state vector would complicate the inversion. We view R instead as an adjustable forward model parameter and conduct simulations with different values of R over the range [0, 1]. The optimum value of R is then selected as that providing the best fit between the observations and the forward model using a posteriori source estimates. The quality of the fit is measured by the χ^2 statistic:

$$\chi^2 = \frac{1}{m-n}\sum_{i=1}^{m}\left[\frac{y_{i,M}-y_i}{\sigma_i}\right]^2, \qquad (7)$$

where $y_{i,M}$ is the forward model value corresponding to observation y_i and $\sigma_i = 0.5\ y_i$ is the observational error as previously discussed. Values of χ^2 are 1.3 using the a priori sources and 0.42–0.62 using the a posteriori sources with varying R (Figure 10). Thus the inversion analysis improves substantially the ability of the forward model to reproduce the observations. The best fit ($\chi^2 = 0.42$) is obtained for R values in the range 0.7–0.85, as shown in Figure 10.

[43] The limitations of our inversion analysis must be acknowledged. First, there is some arbitrariness in the partitioning of the observations into $m = 142$ elements and in the assumption of a 50% observational error. Second, there is no justification (other than lack of information) for ignoring error covariances between observation elements, i.e., for setting the off-diagonal terms of $\mathbf{S}_\epsilon$ to zero. Third, a central assumption in the least squares fitting is that the observations are unbiased, but calibration problems are a concern [*Apel et al.*, 1998]. Fourth, using the χ^2 statistic as a test of model success assumes that the observations are representative of the global acetone concentration field, but in fact, Europe accounts for over half of the observation vector, and there are no observations in the extratropical Southern Hemisphere. We did verify in a series of tests that the inversion provides stable results, and these tests are described in detail by *Jin* [2001]. One test was to use model results with a priori sources as pseudodata for the measurement points in Table 2; the inversion was then conducted starting from perturbed sources to verify convergence to the true a priori values. Additional tests included doubling the weight of the aircraft observations, reducing the assumed errors, and removing different components of the state and observational vectors. Results were stable in all cases.

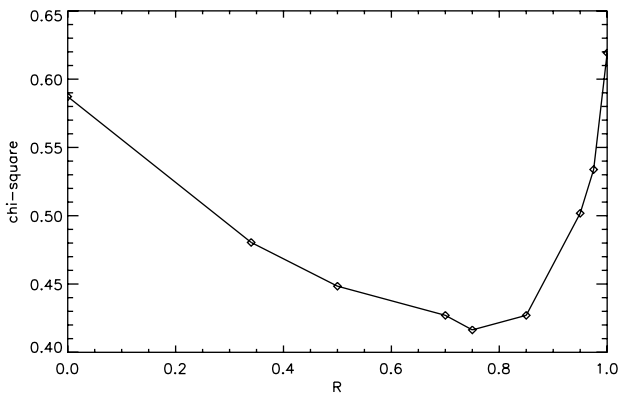

Figure 10. Goodness-of-fit statistic χ^2 (equation (7)) to the ensemble of acetone observations in Table 2 for the forward model using a posteriori source estimates obtained with different values of the ocean saturation ratio R. The forward model using the a priori source estimates and no ocean sink ($R = 1$) yields $\chi^2 = 1.3$.

5. A Posteriori Budgets and Comparisons to Observations

[44] Our best a posteriori estimates of the global acetone source terms are listed in Table 1 for the forward model with an ocean sink corresponding to a saturation ratio $R = 0.85$. As seen from Figure 10, the forward model with $R = 0.7$ would provide as good a fit to the observations as $R = 0.85$; the corresponding range of a posteriori sources lies within the errors in Table 1. The evolution of the state vector over the course of the sequential updating procedure, shown in Figure 11 for the forward model with $R = 0.85$, illustrates how different observations modify the a priori. Before discussing the a posteriori budget and its robustness, however, we first examine in this section the ability of the forward model to match observations using either the a priori source estimates (with $R = 1$) or the a posteriori source estimates (with $R = 0.85$).

5.1. Surface Sites

5.1.1. European sites. [45] Figure 7 compares simulated and observed seasonal variations of acetone concentrations at the nine nonurban European sites of *Solberg et al.* [1996]. The observations have summer maxima and winter minima except at Ispra, where the seasonal variation is reversed, and at Zeppelin (Arctic site), where this is no seasonal variation over the April–September measurement period. The a priori simulation in Figure 7 captures the observed summer maxima and reproduces qualitatively the observed seasonal variation (except at Ispra, which we dismiss as anomalous). The simulated concentrations are too high in the fall and winter months, tend to be too low in the spring months, and are too high at the Zeppelin site. The a posteriori simulation is much better.

[46] The seasonal variation of acetone at the European sites provides complex information on the acetone budget terms. To illustrate this point, in Figure 12 we show the contributions from individual a priori sources to simulated concentrations at Kosetice (Czech Republic) and Birkenes (southern Norway). The most important sources at both sites are oxidation of isoalkanes, vegetative emission, oxidation of monoterpenes, plant decay, and anthropogenic emission. Anthropogenic emission is an important source in winter but is less important in summer; unlike other sources it has no seasonal variation, and its effect in summer is depressed by vertical mixing and photochemical loss. Oxidation of isoalkanes, propane being the most important, is a major source year-round with a broad spring maximum. Plant decay peaks in early fall when litter is abundant and temperatures are high. Vegetative emissions are largely confined to June–September and play a critical role in defining the summer maximum. Birkenes is more remote, less continental, and farther north than Kosetice so that the acetone concentrations are lower, the contribution from oxidation of isoalkanes is relatively larger, the industrial and biogenic sources are smaller, and monoterpenes make a relatively greater contribution to the biogenic source.

[47] Most of the constraint on the ocean sink in our analysis is driven by the seasonal variation at the European sites and by the low values at the Zeppelin Arctic site in April–September, as shown in Figure 7. In order to capture the winter minima at the European sites we need an ocean sink and a reduction of the plant decay source (Figure 11). This adjustment not only captures the winter minima but also improves the simulation of the seasonal increase from winter to spring and the seasonal decrease from summer to fall. Inclusion of the ocean sink allows the model to match the Zeppelin observations.

5.1.2. North American sites. [48] Figure 8 compares model results to summertime observations at four nonurban sites in eastern North America (Table 2). The model reproduces the mean concentrations of 1.5–2 ppbv observed at Mettler (Georgia) and Dorset/Egbert (Ontario) but not the much higher values observed at Kinterbish (Alabama) and Youth, Inc. (Tennessee). These

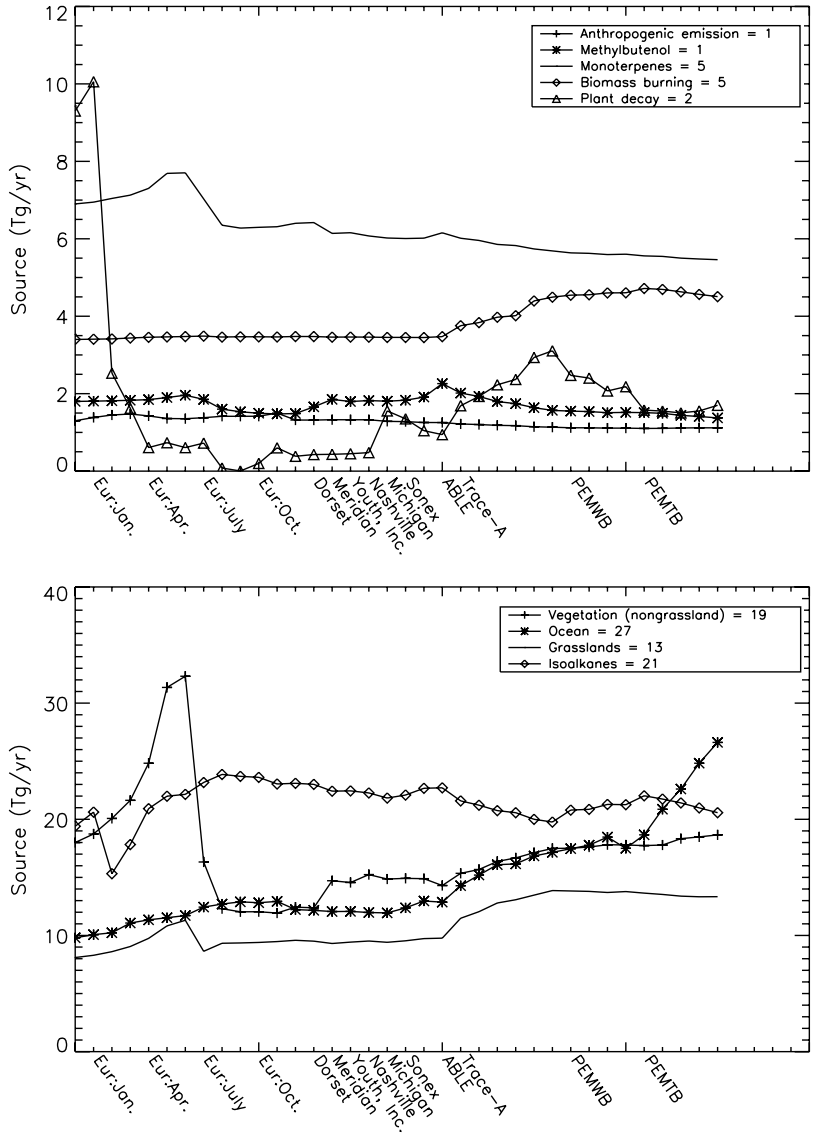

Figure 11. Update of state vector elements (global acetone source terms) from the sequential application of observation subvectors in the inversion analysis. The sequence of application is shown on the *x* axis. The ordinate values for the left and right ends of each curve represent the a priori and a posteriori source estimates, respectively.

extremely high concentrations have a clear biogenic signature in the observations [*Goldan et al.*, 1995; *Riemer et al.*, 1998]. The model source of acetone over eastern North America in summer is overwhelmingly biogenic (Figure 8) but cannot be adjusted in the inversion in a way that would improve the simulation consistently at all four sites. Considering the long acetone lifetime and hence the expected regional homogeneity of its distribution, the only way to reconcile the high observations at Kinterbish and Youth, Inc. with the much lower values at nearby Mettler is if the first two sites are affected by an unusually large local vegetation source.

[49] An extensive record of summertime acetone concentrations, canopy-scale fluxes, and ancillary chemical tracer data is available from the Blodgett Forest mountain slope site in the California Sierra Nevada (39°N, 121°W, 1300 m elevation). The mean measured acetone concentration in July is 4.3 ppbv [*Lamanna and Goldstein*, 1999]. Using correlations with chemical tracers and other information, *Goldstein and Schade* [2000] apportioned the observed acetone at the site as 14% from secondary anthropogenic sources in the California Central Valley, 28% from oxidation of methylbutenol, 16% from direct emission by vegetation and soils, 1% from oxidation of monoterpenes, and 41% from regional background. Measurements at mountain slope sites are affected by shallow orographic circulations and inversions and are thus poorly suited for comparison to a global model, but it is nevertheless of interest to compare the source apportionments. We find in the model a mean July concentration of 1.6 ppbv at the Blodgett Forest site reflecting source contributions of 40% from oxidation of methylbutenol, 25% from vegetative emission, 10% from soil emission (plant decay), 15% from oxidation of monoterpenes, and 10% from oxidation of (anthropogenic) isoalkanes. This source apportionment is, in fact, not inconsistent with that of *Goldstein and Schade* [2000], since they point out that their "anthropogenic" contribution would include biogenic sources such as from monoterpenes transported to the site together with the Central Valley pollution plume. Our simulated mean acetone concentration matches their diagnosed regional background, although one would expect from the model an enhancement above background unless the enhancements seen in the observations were highly localized.

[50] Also shown in Figure 8 are comparisons of model results to January observations at a rural Michigan site [*Couch et al.*, 2000]

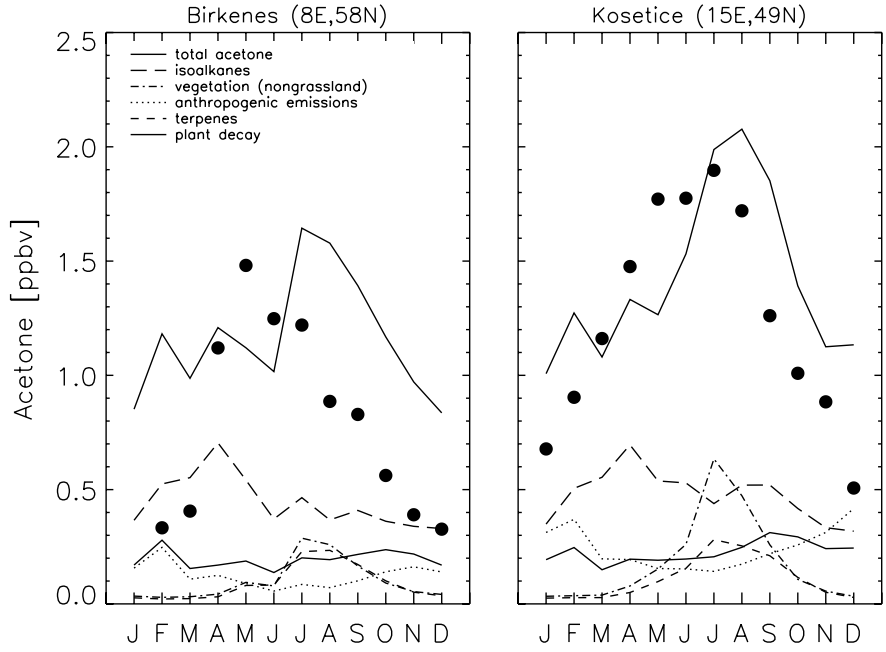

Figure 12. Contributions from different a priori source terms to the simulated seasonal variation of acetone concentrations at Birkenes (southern Norway) and Kosetice (Czech Republic). All values are monthly means. Observations are shown as symbols.

and to April observations at the Arctic site of Alert [*Bottenheim et al.*, 1990; *Shepson et al.*, 1996; *Yokouchi et al.*, 1994]. We have excluded the Alert observations made during local halogen-catalyzed ozone depletion events, when acetone concentrations are found to increase presumably because of fast oxidation of isoalkanes by Cl atoms [*Yokouchi et al.*, 1994]. The Alert observations span a wide range (0.39–1.5 ppbv), and their quality is uncertain; therefore we have not used them in the inversion. Both the a priori and a posteriori simulations are consistent with the Michigan and Alert observations; the dominant sources of acetone in the model at both sites are oxidation of isoalkanes and plant decay. As mentioned in section 2.3, recent observations at Alert suggest that exchange with the snowpack plays an important role in determining local acetone concentrations.

5.2. Aircraft Observations

5.2.1. North Atlantic (SONEX). [51] Simulated vertical profiles over the North Atlantic in October are compared in Figure 9 to observations from the SONEX mission. Oxidation of isoalkanes is the single most important source of acetone for that region and season, contributing ~0.4 ppbv near the surface and ~0.2 ppbv in the upper troposphere; plant decay is the next largest source. Both the a priori and a posteriori simulations closely match the observed concentrations in the upper troposphere, where the bulk of the measurements were taken. The a posteriori concentrations in the lower troposphere are smaller than the a priori because of the ocean sink, but no observations were made there.

5.2.2. Eastern Canada (ABLE-3B). [52] Measurements of acetone concentrations up to 6 km altitude were made during the ABLE-3B mission over eastern Canada in summer. The a priori simulation underestimates the free tropospheric concentrations by 30%, with less bias in the boundary layer; the a posteriori simulation shows little difference from the a priori. The most important sources of acetone for that region in the model are oxidation of methylbutenol, monoterpenes, and isoalkanes, in that order. The first two sources are responsible for the boundary layer enhancement. Previous analyses of the ABLE-3B data using correlations with chemical tracers showed that forest fires were a major contributor to acetone in the free troposphere [*Singh et al.*, 1994; *Wofsy et al.*, 1994]. In our model this source is small, contributing only 0.05–0.1 ppbv. *Singh et al.* [1994] reported an acetone/CO molar emission ratio of 2.5% mol mol^{-1} for the biomass burning plumes sampled in ABLE-3B, which is 1 order of magnitude higher than the mean biomass burning emission ratio from the compilation of *Andreae and Merlet* [2001] and was, in fact, rejected from that compilation for being anomalously high (M. O. Andreae, personal communication, 2001). The acetone/CO molar ratios measured in ABLE-3B could have included contributions from chemical production of acetone within the biomass burning plumes [*Singh et al.*, 1994]. However, our simulation of the TRACE-A observations where biomass burning also had a large influence does not show a similar underestimate of acetone (Figure 9).

5.2.3. Western Pacific (PEM-West B). [53] Measurements of acetone up to 12 km altitude were made in the PEM-West B mission over the western Pacific in February–March 1994, the same meteorological year as the model. A major feature of observations is the strong Asian outflow north of 20°N below 6 km altitude. The a priori simulation overestimates the acetone enhancement in this outflow but the a posteriori simulation corrects this discrepancy through the ocean sink. Oxidation of isoalkanes contributes over half of the model acetone in the midlatitude profiles (Japan coast, southeast China, midwest Pacific). For the west tropical Pacific region, oxidation of isoalkanes and oceanic emission make comparable contributions.

5.2.4. South Atlantic (TRACE-A). [54] The TRACE-A mission over Brazil, southern Africa, and the South Atlantic in September–October sampled an atmosphere heavily affected by seasonal biomass burning [*Fishman et al.*, 1996]. The model underestimates observations in region 12 (active fire region in southern Africa) but provides a good simulation elsewhere. Biomass burning is the dominant source of acetone in the model over southern Africa and the African west coast below 6 km; the TRACE-A observations increase that source slightly in the a posteriori simulation (Figure 9).

[55] The principal model sources of acetone over Brazil and in the free troposphere over the South Atlantic are from terrestrial vegetation, with comparable contributions from grassland and nongrassland ecosystems. There is little difference between the a priori and a posteriori simulations. In the marine boundary layer over the South Atlantic the single most important source of acetone is photochemical production in the ocean. This source increases in the a posteriori simulation to compensate for the ocean sink so that there is again little change in the simulated concentrations.

5.2.5. Tropical Pacific (PEM-Tropics B). [56] Measurements from the PEM-Tropics B mission over the tropical Pacific in March–April offer particularly extensive geographical coverage from 30°N to 30°S and from the surface to 12 km altitude. Concentrations decrease slightly from the northern to the southern tropical Pacific and show little variation with altitude in either hemisphere. The model reproduces closely the observations over Hawaii, the equatorial Pacific, Fiji, and Tahiti (a posteriori); it is too low in the free troposphere over Easter Island. Oxidation of isoalkanes is the principal model source of acetone over Hawaii, contributing about half the total. The ocean source dominates in the other regions, accounting for up to half of total acetone at Tahiti and Easter Island. Grasslands are also an important contributor over Fiji.

[57] The a posteriori simulation of the PEM-Tropics B data yields higher concentrations over the South Pacific than the a priori simulation and provides a better match to observations. Application of the PEM-Tropics B data in the inversion analysis imposes a large increase in the photochemical ocean source in order to balance the ocean sink required by the European observations (Figure 11). The ocean source in the model imposes a gradient of decreasing concentrations from the marine boundary layer to the free troposphere, but this gradient is only marginally apparent in the observations (and is actually reversed over Easter Island). A vertically distributed source over the South Pacific, perhaps from marine organic aerosol, would better fit the observations.

6. Comparison of A Priori and A Posteriori Budgets

[58] The global a posteriori source of acetone given in Table 1 (95 ± 15 Tg yr^{-1}) is 22% larger than the a priori source (78 ± 27 Tg yr^{-1}), mostly because of the increase in the ocean source. The errors given for the a posteriori terms are the square roots of the diagonal terms of $\hat{\mathbf{S}}$, but the actual errors are certainly higher because of unresolved biases and correlations in the observations. Sensitivity tests of the inversion method in which a priori or observational errors are reduced by a factor of 2, or in which individual sources or observation elements are removed from the inversion, indicate that the a posteriori results in Table 1 are generally stable within the stated errors [*Jin*, 2001]. We conducted an eigenvalue decomposition of $\hat{\mathbf{S}}$ to identify major error patterns. We find that the error on the nongrassland vegetation source is negatively correlated with the error on the grassland source, indicating that errors on these two sources tend to compensate each other. In a calculation in which the grassland and nongrassland vegetation sources were combined, we obtained a total source from terrestrial vegetation of 33 ± 9 Tg yr^{-1}, identical to the sum of the two components but with less relative error.

[59] The most dramatic difference between the a priori and a posteriori budgets of acetone is the role of the ocean. The strong ocean sink in the a posteriori budget (14 Tg yr^{-1}) is needed to capture the seasonal cycle of concentrations observed at European sites as well as the low spring-summer concentrations at the Zeppelin Arctic site. The effect of this sink is compensated in the tropics by a large photochemical ocean source (27 Tg yr^{-1}). On a global basis the ocean provides a net source of 13 Tg yr^{-1} of acetone in the a posteriori budget, which is comparable to 10 Tg yr^{-1} in the a priori. However, this net global source now represents a balance between a net ocean sink at high latitudes in winter and a net ocean source in the tropics. Measurements at

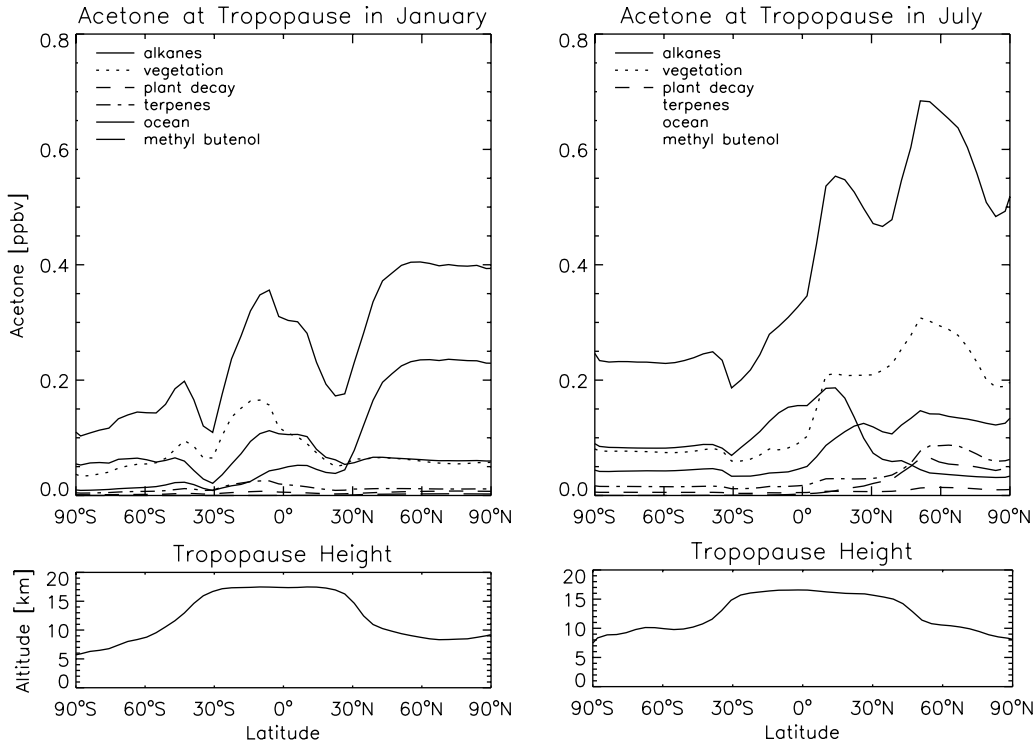

Figure 13. Contributions fron different sources to the acetone concentrations just below the tropopause in January and July for the simulation with a posteriori sources. Values are monthly means. The bold line shows total acetone. "Vegetation" includes contributions from both grassland and nongrassland terrestrial vegetation types. Monthly mean tropopause heights from the GEOS data are also shown.

high southern latitudes in winter would provide a sensitive test of the ocean sink hypothesis, as the atmospheric distribution constructed from the a posteriori budget predicts concentrations of <200 pptv in that region (Figure 5).

[60] The a posteriori source of acetone from isoalkanes (21 ± 5 Tg yr^{-1}) is little changed from the a priori source, but the error is reduced. Oxidation of isoalkanes is a major source of acetone for most of the observational data sets used in the inversion, and the a priori source appears to offer a good simulation of the observations. We tried to separate propane from the higher isoalkanes in the inversion analysis but were unsuccessful because of excessive overlap. On the basis of our discussion in section 2.2, propane is the principal contributor to the isoalkane source.

[61] The a posteriori source of acetone from grasslands (13 ± 7 Tg yr^{-1}) is 60% greater than the a priori value, while the a posteriori source from other terrestrial vegetation (19 ± 9 Tg yr^{-1}) is similar to the a priori. In both cases the relative error is reduced to ~50%. The change in the grassland source estimate is determined largely by the TRACE-A observations.

[62] The a posteriori source from plant decay (2 ± 5 Tg yr^{-1}) is a factor of 3 less than the a priori, although the range of error covers both the a priori value and negative values (negative values correspond to surface uptake, i.e., an increase in the 9 Tg yr^{-1} sink from dry deposition to land already included in the forward model). The decrease of the plant decay source in the inversion analysis is driven largely by the European observations, specifically the low winter-spring values and the rapid decrease from summer to fall. Although the laboratory data of *Warneke et al.* [1999] demonstrate acetone production during the abiotic decay of vegetation, this acetone could be consumed within the litter rather than emitted to the atmosphere. *Schade and Goldstein* [2001] observed soil emission of acetone at the Blodgett Forest site but pointed out that the local dry climate would be particularly conducive to acetone escape from the litter.

[63] Acetone is of particular chemical interest just below the tropopause where it may provide the dominant source of HO_x radicals and drive rapid ozone production [*Wennberg et al.*, 1998; *Jaeglé et al.*, 2001]. In Figure 13 we show the simulated contributions from the different a posteriori sources to acetone concentrations in the GEOS-CHEM model level just below the tropopause (GEOS tropopause heights are also indicated). In the tropics and the Southern Hemisphere the principal sources are from terrestrial vegetation and the ocean. In the extratropical Northern Hemisphere, oxidation of isoalkanes dominates in winter, but the terrestrial biosphere becomes important in summer, resulting in particularly high acetone concentrations (>0.5 ppbv). Increasing production of natural gas in the future could have a major impact on acetone at the tropopause.

7. Conclusion

[64] We have evaluated our current understanding of the atmospheric budget of acetone by constructing best a priori estimates of acetone sources and sinks for use in a global 3-D model and comparing model results to acetone concentrations observed from surface sites and aircraft. An inversion analysis was used to explore the constraints offered by the atmospheric observations toward improving the definition of acetone sources and sinks.

[65] The C_3–C_5 isoalkanes (propane, isobutane, isopentane) represent major atmospheric precursors of acetone and are simulated explicitly in the model. Their sources are almost exclusively anthropogenic, and we compared simulated concentrations to atmospheric observations worldwide to improve source estimates. We found that the EDGAR V2.0 emission inventory greatly underestimates the atmospheric observations of propane and isobutane at northern midlatitudes. Our best estimate of global emissions is 12 Tg C yr^{-1} for propane (including only 0.6 Tg C yr^{-1} from biomass burning), 3.6 Tg C yr^{-1} for isobutane, and 5.0 Tg C yr^{-1} for isopentane. Propane concentrations in the Southern Hemisphere appear to be dominated by natural gas emissions rather than by biomass burning.

[66] Exchange with the ocean must be considered in the budget of atmospheric acetone, if only because the solubility of acetone in seawater is sufficiently high to represent an important sink for atmospheric acetone unless there is a reverse flux. The oceans provide both a photochemical source and a microbial sink of acetone. Matching the aircraft observations of 0.4 ppbv acetone over the South Pacific requires a large photochemical ocean source which could be supplied by either surface emission or production within the atmosphere from marine organic aerosols. Matching surface observations at European sites in winter and also the observed latitudinal gradient between Europe and the Arctic in spring-summer suggests a large microbial ocean sink corresponding to an acetone saturation ratio in the ocean in the range 0.7–0.85. Measurements of the saturation ratio of acetone in the ocean are needed to better constrain the role of the ocean in the atmospheric budget of acetone.

[67] Abiotic reactions during plant decay have been proposed as a potentially large source of acetone to the atmosphere [*Warneke et al.*, 1999], but such a source appears to be inconsistent with the seasonal cycle observed at European sites, including the low concentrations in winter-spring and the rapid decrease from summer to fall. It may be that the acetone produced in plant decay is consumed within the surface litter rather than emitted to the atmosphere.

[68] Large sources of acetone from terrestrial vegetation and from atmospheric oxidation of isoalkanes are confirmed by our analysis. The terrestrial vegetation source is responsible for the high acetone concentrations observed over the tropical continents and at continental sites in northern midlatitudes in summer. The source from atmospheric oxidation of isoalkanes is important for explaining the acetone concentrations observed in the extratropical Northern Hemisphere outside of summer. Our simple specification of acetone vegetative emissions in the model is unable to reproduce local observations of very high acetone concentrations at U.S. sites in summer. Better understanding of these vegetative emissions is evidently needed.

[69] Our best estimate of the global source of acetone is 95 Tg yr^{-1} including 33 Tg yr^{-1} from terrestrial vegetation, 27 Tg yr^{-1} from the oceans, 21 Tg yr^{-1} from atmospheric oxidation of isoalkanes (mostly propane), 6 Tg yr^{-1} from atmospheric oxidation of monoterpenes, 5 Tg yr^{-1} from biomass burning, 2 Tg yr^{-1} from plant decay, 1 Tg yr^{-1} from atmospheric oxidation of methylbutenol, and 1 Tg yr^{-1} from anthropogenic emission (solvent use and automobiles). Our best estimate of the lifetime of acetone in the troposphere is 15 days with photolysis contributing 45% of the sink, oxidation by OH 30%, ocean uptake 15%, and dry deposition to land 10%. Simulated concentrations of acetone just below the tropopause (0.1–0.7 ppbv) are mostly of vegetative and oceanic origin, except in the extratropical Northern Hemisphere in winter where oxidation of isoalkanes is a major source.

[70] **Acknowledgments.** Comments from Allen Goldstein and Prasad Kasibhatla are gratefully acknowledged. This work was supported by the National Science Foundation (NSF-ATM) and by the National Aeronautics and Space Administration (NASA-ACMAP). H. B. Singh acknowledges support from the NASA IDS program.

References

Alvarado, A., E. C. Tuazon, S. M. Aschmann, J. Arey, and R. Atkinson, Products and mechanisms of the gas-phase reactions of OH radicals and O_3 with 2-methyl-3-buten-2-ol, *Atmos. Environ.*, *33*, 2893–2905, 1999.

Andreae, M. O., and P. Merlet, Emission of trace gases and aerosols from biomass burning, *Global Biogeochem. Cycles*, *15*, 955–966, 2001.

Apel, E. C., et al., Measurements comparison of oxygenated volatile organic compounds at a rural site during the 1995 SOS Nashville Intensive, *J. Geophys. Res.*, *103*, 22,295–22,316, 1998.

Arnold, F., V. Burger, B. Droste-Fanke, F. Grimm, A. Krieger, J. Schneider, and T. Stilp, Acetone in the upper troposphere and lower stratosphere: Impact on trace gases and aerosols, *Geophys. Res. Lett.*, *24*, 3017–3020, 1997.

Atkinson, R., Gas-phase tropospheric chemistry of volatile organic compounds, 1, Alkanes and alkenes, *J. Phys. Chem. Ref. Data*, *26*, 215–290, 1997.

Baker, B., A. Guenther, J. Greenberg, A. Goldstein, and R. Fall, Canopy fluxes of 2-methyl 3-buten-2-ol over a ponderosa pine forest by relaxed eddy accumulation: Field data and model comparison, *J. Geophys. Res.*, *104*, 26,107–26,114, 1999.

Bey, I., D. J. Jacob, R. M. Yantosca, J. A. Logan, B. Field, A. M. Fiore, Q. Li, H. Liu, L. J. Mickley, and M. Schultz, Global modeling of tropospheric chemistry with assimilated meteorology: Model description and evaluation, *J. Geophys. Res.*, *106*, 23,073–23,095, 2001.

Blake, D. R., and F. S. Rowland, Urban leakage of liquefied petroleum gas and its impact on Mexico City air quality, *Science*, *269*, 953–956, 1995.

Blake, D. R., D. F. Hurst, T. W. Smith Jr., W. J. Whipple, T.-Y. Chen, N. J. Blake, and F. S. Rowland, Summertime measurements of selected nonmethane hydrocarbons in the Arctic and Subarctic during the 1988 Arctic Boundary Layer Expedition (ABLE 3A), *J. Geophys. Res.*, *97*, 16,559–16,588, 1992.

Blake, D. R., T. W. Smith Jr., T.-Y. Chen, W. J. Whipple, and F. S. Rowland, Effects of biomass burning on summertime nonmethane hydrocarbon concentrations in the Canadian wetlands, *J. Geophys. Res.*, *99*, 1699–1720, 1994.

Blake, N. J., D. R. Blake, B. C. Sive, T. Chen, F. S. Rowland, J. E. Collins Jr., G. W. Sachse, and B. E. Anderson, Biomass burning emissions and vertical distribution of methyl halides and other reduced carbon gases in the South Atlantic region, *J. Geophys. Res.*, *101*, 24,151–24,164, 1996.

Blake, N. J., D. R. Blake, T.-Y. Chen, J. E. Collins, Jr., G. W. Sachse, B. E. Anderson, and F. S. Rowland, Distribution and seasonality of selected hydrocarbons and halocarbons over the western Pacific basin during PEM-West A and PEM-West B, *J. Geophys. Res.*, *102*, 28,315–28,331, 1997.

Blake, N. J., et al., Influence of southern hemispheric biomass burning on midtropospheric distributions of nonmethane hydrocarbons and selected halocarbons over the remote South Pacific, *J. Geophys. Res.*, *104*, 16,213–162,32, 1999.

Blake, N. J., et al., Large-scale latitudinal and vertical distributions of NMHCs and selected halocarbons in the troposphere over the Pacific Ocean during the March–April 1999 Pacific Exploratory Mission (PEM Tropics B), *J. Geophys. Res.*, *106*, 32,627–32,644, 2001.

Blough, N. V., Photochemistry in the sea-surface microlayer, in *The Sea Surface and Global Change*, edited by P. S. Liss and R. A. Duce, pp. 383–424, Cambridge Univ. Press, New York, 1997.

Bottenheim, J. W., L. A. Barrie, E. Atlas, L. E. Heidt, H. Niki, R. A. Rasmussen, and P. B. Shepson, Depletion of lower tropospheric ozone during Arctic spring: The Polar Sunrise Experiment 1988, *J. Geophys. Res.*, *95*, 18,555–18,568, 1990.

Brasseur, G. P., D. A. Hauglustaine, S. Walters, P. J. Rasch, J.-F. Muller, C. Granier, and X. X. Tie, MOZART, a global chemical transport model for ozone and related chemical tracers, 1, Model description, *J. Geophys. Res.*, *103*, 28,265–28,289, 1998.

Cameron-Smith, P. J., Incorporation of non-linear cross-sections into a fast photolysis computation code (Fast-J), *J. Atmos. Chem.*, *37*, 283–297, 2000.

Chatfield, R. B., E. P. Gardner, and J. G. Calvert, Sources and sinks of acetone in the troposphere: Behavior of reactive hydrocarbons and a stable product, *J. Geophys. Res.*, *92*, 4208–4216, 1987.

Clarkson, T. S., R. J. Martin, and J. Rudolph, Ethane and propane in the southern marine troposphere, *Atmos. Environ.*, *31*, 3763–3771, 1997.

Collins, W. J., D. S. Stevenson, C. E. Johnson, and R. G. Derwent, Role of convection in determining the budget of odd hydrogen in the upper troposphere, *J. Geophys. Res.*, *104*, 26,927–26,941, 1999.

Couch, T. L., A. L. Sumner, T. M. Dassau, and P. B. Shepson, An investigation of the interaction of carbonyl compounds with the snowpack, *Geophys. Res. Lett.*, *27*, 2241–2244, 2000.

Duncan, B. N., R. V. Martin, A. C. Staudt, R. M. Yevich, and J. A. Logan, Interannual and seasonal variability of biomass burning emissions constrained by remote-sensed observations, paper presented at International Workshop on Emissions of Chemical Species and Aerosols into the Atmosphere, Global Emiss. Invent. Activ. of the Int. Global Atmos. Chem. Program, Paris, France, 19–22 June 2001.

Fall, R., Biogenic emissions of volatile organic compounds from higher plants, in *Reactive Hydrocarbons in the Atmosphere*, edited by C. N. Hewitt, pp. 41–96, Academic, San Diego, Calif., 1999.

Ferek, R. J., J. S. Reid, P. V. Hobbs, D. R. Blake, and C. Liousse, Emision factors of hydrocarbons, halocarbons, trace gases and particles from biomass burning in Brazil, *J. Geophys. Res.*, *103*, 32,107–32,118, 1998.

Fishman, J., J. M. Hoell Jr., R. D. Bendura, R. J. McNeal, and V. W. J. H. Kirchhoff, NASA GTE TRACE A Experiment (September–October 1992): Overview, *J. Geophys. Res.*, *101*, 23,865–23,880, 1996.

Gierczak, T., J. B. Burkholder, S. Bauerle, and A. R. Ravishankara, Photochemistry of acetone under tropospheric conditions, *Chem. Phys.*, *231*, 229–244, 1998.

Goldan, P. D., W. C. Kuster, F. C. Fehsenfeld, and S. A. Montzka, Hydrocarbon measurements in the southeastern United States: The Rural Oxidants in the Southern Environment (ROSE) program 1990, *J. Geophys. Res.*, *100*, 35,945–35,963, 1995.

Goldan, P. D., D. D. Parrish, W. C. Kuster, M. Trainer, S. A. McKeen, J. Holloway, B. T. Jobson, D. T. Sueper, and F. C. Fehsenfeld, Airborne measurements of isoprene, CO, and anthropogenic hydrocarbons and their implications, *J. Geophys. Res.*, *105*, 9091–9105, 2000.

Goldstein, A. H., and G. W. Schade, Quantifying biogenic and anthropogenic contributions to acetone mixing ratios in a rural environment, *Atmos. Environ.*, *34*, 4997–5006, 2000.

Goldstein, A. H., S. C. Wofsy, and C. M. Spivakovsky, Seasonal variations of nonmethane hydrocarbons in rural New England: Constraints on OH concentrations in northern midlatitudes, *J. Geophys. Res.*, *100*, 21,023–21,033, 1995.

Grannas, A. M., A study of photochemical and physical processes affecting carbonyl compounds in the Arctic atmospheric boundary layer, *Atmos. Environ.*, in press, 2002.

Guenther, A., et al., A global model of natural volatile organic compound emissions, *J. Geophys. Res.*, *100*, 8873–8892, 1995.

Guenther, A., C. Geron, T. Pierce, B. Lamb, P. Harley, and R. Fall, Natural emissions of non-methane volatile organic compounds, carbon monoxide, and oxides of nitrogen from North America, *Atmos. Environ.*, *34*, 2205–2230, 2000.

Guimbaud, C., et al., Snowpack processing of acetaldehyde and acetone in the Arctic atmospheric boundary layer, *Atmos. Environ.*, in press, 2002.

Gupta, M. L., R. J. Cicerone, D. R. Blake, F. S. Rowland, and I. S. A. Isaksen, Global atmospheric distributions and source strengths of light hydrocarbons and tetrachloro-ethene, *J. Geophys. Res.*, *103*, 28,219–28,235, 1998.

Harley, P., V. Fridd-Stroud, J. Greenberg, A. Guenther, and P. Vasconcellos, Emission of 2-mthyl-3-buten-2-ol by pines: A potentially large natural source of reactive carbon to the atmosphere, *J. Geophys. Res.*, *103*, 25,479–25,486, 1998.

Hauglustaine, D. A., G. P. Brasseur, S. Walters, P. J. Rasch, J.-F. Muller, L. K. Emmons, and M. A. Carroll, MOZART, a global chemical transport model for ozone and related chemical tracers, 2, Model results and evaluation, *J. Geophys. Res.*, *103*, 28,291–28,335, 1998.

Jacob, D. J., et al., Origin of ozone and NO_x in the tropical troposphere: A photochemical analysis of aircraft observations over the South Atlantic Basin, *J. Geophys. Res.*, *101*, 24,235–24,250, 1996.

Jaeglé, L., et al., Observations of OH and HO_2 in the upper troposphere suggest a strong source from convective injection of peroxides, *Geophys. Res. Lett.*, *24*, 3181–3184, 1997.

Jaeglé, L., D. J. Jacob, W. H. Brune, and P. O. Wennberg, Chemistry of HO_x radicals in the upper troposphere, *Atmos. Environ.*, *35*, 469–489, 2001.

Jin, E. M., Determining global acetone emissions using an inverse method, senior thesis, Harvard Univ., Cambridge, Mass., 2001.

Jobson, B. T., Z. Wu, H. Niki, and L. A. Barrie, Seasonal trends of isoprene, C_2–C_5 alkanes, and acetylene at a remote boreal forest site in Canada, *J. Geophys. Res.*, *99*, 1589–1599, 1994.

Kieber, R. J., X. Zhou, and K. Mopper, Formation of carbonyl compounds from UV-induced photodegradation of humic substances in natural waters: Fate of riverine carbon in the sea, *Limnol. Oceanogr.*, *35*, 1503–1515, 1990.

Kirstine, W., I. Galbally, Y. Ye, and M. Hooper, Emissions of volatile organic compounds (primarily oxygenated species) from pasture, *J. Geophys. Res.*, *103*, 10,605–10,619, 1998.

Lamanna, M. S., and A. H. Goldstein, In situ measurements of C_2–C_{10} volatile organic compounds above a Sierra Nevada ponderosa pine plantation, *J. Geophys. Res.*, *104*, 21,247–21,262, 1999.

Lee, Y.-N., X. Zhou, and K. Hallock, Atmospheric carbonyl compounds at a rural southeastern United States site, *J. Geophys. Res.*, *100*, 25,933–25,944, 1995.

Liss, P. S., Processes of gas exchange across an air-water interface, *Deep Sea Res.*, *20*, 221–228, 1973.

Liss, P. S., and P. G. Slater, Flux of gases across the air-sea interface, *Nature*, *247*, 181–184, 1974.

Madronich, S., and J. G. Calvert, The NCAR master mechanism of the gas phase chemistry, Version 2.0, *NCAR Tech. Note NCAR/TN-333+STR*, 1989.

Mauzerall, D. L., J. A. Logan, D. J. Jacob, B. E. Anderson, D. R. Blake,

J. D. Bradshaw, B. Heikes, G. W. Sachse, H. B. Singh, and R. W. Talbot, Photochemistry in biomass burning plumes and implications for tropospheric ozone over the tropical South Atlantic, *J. Geophys. Res.*, *103*, 8401–8424, 1998.

McKeen, S. A., T. Gierczak, J. B. Burkholder, P. O. Wennberg, T. F. Hanisco, E. R. Keim, R.-S. Gao, S. C. Liu, A. R. Ravishankara, and D. W. Fahey, The photochemistry of acetone in the upper troposphere: A source of odd-hydrogen radicals, *Geophys. Res. Lett.*, *24*, 3177–3180, 1997.

Middleton, P., W. R. Stockwell, and W. P. L. Carter, Aggregation and analysis of volatile organic compound emissions for regional modeling, *Atmos. Environ., Part A*, *24*, 1107–1133, 1990.

Müller, J.-F., and G. Brasseur, Sources of upper tropospheric HO_x: A three-dimensional study, *J. Geophys. Res.*, *104*, 1705–1715, 1999.

Nightingale, P. D., G. Malin, C. S. Law, A. J. Watson, P. S. Liss, M. I. Liddicoat, J. Boutin, and R. C. Upstill-Goddard, In situ evaluation of air-sea gas exchange parameterizations using novel conservative and volatile tracers, *Global Biogeochem. Cycles*, *14*, 373–387, 2000.

Olivier, J. G. J., A. F. Bouwman, C. W. M. Van der Maas, and J. J. M. Berdowski, Emission Database for Global Atmospheric Research (EDGAR), *Environ. Monit. Assessment*, *31*, 93–106, 1994.

Olson, J., World ecosystems (WE1.4): Digital raster data on a 10 minute geographic 1080x2160 grid, in *Global Ecosystems Database*, version 1.0, NOAA Natl. Geophys. Data Cent., Boulder, Colo., 1992.

Orlando, J. J., B. Noziere, G. S. Tyndall, G. E. Orzechowska, S. E. Paulson, and Y. Rudich, Product studies of the OH- and ozone-initiated oxidation of some monoterpenes, *J. Geophys. Res.*, *105*, 11,561–11,572, 2000.

Phadnis, M. J., and G. R. Carmichael, Transport and distribution of primary and secondary nonmethane volatile organic compounds in east Asia under continental outflow conditions, *J. Geophys. Res.*, *105*, 22,311–22,336, 2000.

Piccot, S. D., J. J. Watson, and J. W. Jones, A global inventory of volatile organic compound emissions from anthropogenic sources, *J. Geophys. Res.*, *97*, 9897–9912, 1992.

Plass-Dulmer, C., R. Koppmann, M. Ratte, and J. Rudolph, Light nonmethane hydrocarbons in seawater, *Global Biogeochem. Cycles*, *9*, 79–100, 1995.

Potter, C. S., J. T. Randerson, C. B. Field, P. A. Matson, P. M. Vitousek, H. A. Mooney, and S. A. Klooster, Terrestrial ecosystem production: A process model based on global satellite and surface data, *Global Biogeochem. Cycles*, *7*, 811–841, 1993.

Prinn, R. G., R. F. Weiss, B. R. Miller, J. Huang, F. N. Alyea, D. M. Cunnold, P. J. Fraser, D. E. Hartley, and P. G. Simmonds, Atmospheric trends and lifetime of CH_3CCl_3 and global OH concentrations, *Science*, *269*, 187–192, 1995.

Reissell, A., C. Harry, S. M. Aschmann, R. Atkinson, and J. Arey, Formation of acetone from the OH radical- and O_3-initiated reactions of a series of monoterpenes, *J. Geophys. Res.*, *104*, 13,869–13,879, 1999.

Riemer, D., et al., Observations of nonmethane hydrocarbons and oxygenated volatile organic compounds at a rural site in the southeastern United States, *J. Geophys. Res.*, *103*, 28,111–28,128, 1998.

Rodgers, C. D., *Inverse Methods for Atmospheric Sounding: Theory and Practice*, World Sci., Singapore, 2000.

Saito, T., Y. Yokouchi, and K. Kawamura, Distributions of C_2–C_6 hydrocarbons over the western North Pacific and eastern Indian Ocean, *Atmos. Environ.*, *34*, 4373–4381, 2000.

Schade, G. W., and A. H. Goldstein, Fluxes of oxygenated volatile organic compounds from a ponderosa pine plantation, *J. Geophys. Res.*, *106*, 3111–3123, 2001.

Schneider, H. R., D. B. A. Jones, M. B. McElroy, and G.-Y. Shi, Analysis of residual mean transport in the stratosphere, 1, Model description and comparison with satellite data, *J. Geophys. Res.*, *105*, 19,991–20,011, 2000.

Shepson, P. B., D. R. Hastie, H. I. Schiff, M. Polizzi, J. W. Bottenheim, K. Anlauf, G. I. Mackay, and D. R. Karecki, Atmospheric concentrations and temporal variations of C_1–C_3 carbonyl compounds at two rural sites in central Ontario, *Atmos. Environ., Part A*, *25*, 2001–2016, 1991.

Shepson, P. B., A.-P. Sirju, J. F. Hopper, L. A. Barrie, V. Young, H. Niki, and H. Dryghout, Sources and sinks of carbonyl compounds in the Arctic Ocean boundary layer: Polar Ice Floe Experiment, *J. Geophys. Res.*, *101*, 21,081–21,089, 1996.

Singh, H. B., and P. L. Hanst, Peroxyacetylnitrate (PAN) in the unpolluted atmosphere: An important reservoir for nitrogen oxides, *Geophys. Res. Lett.*, *8*, 941–944, 1981.

Singh, H. B., and P. B Zimmerman, Atmospheric distribution and sources of nonmethane hydrocarbons, in *Gaseous Pollutants: Characterization and Cycling*, edited by J. O. Nriagu, pp. 177–235, John Wiley, New York, 1992.

Singh, H. B., D. O'Hara, D. Herlth, W. Sachse, D. R. Blake, J. D. Bradshaw, M. Kanakidou, and P. J. Crutzen, Acetone in the atmosphere: Distribution, sources, and sinks, *J. Geophys. Res.*, *99*, 1805–1819, 1994.

Singh, H. B., M. Kanakidou, P. J. Crutzen, and D. J. Jacob, High concentrations and photochemical fate of oxygenated hydrocarbons in the global troposphere, *Nature*, *378*, 50–54, 1995.

Singh, H., et al., Distribution and fate of selected oxygenated organic species in the troposphere and lower stratosphere over the Atlantic, *J. Geophys. Res.*, *105*, 3795–3806, 2000.

Singh, H. B., Y. Chen, A. C. Staudt, D. J. Jacob, D. R. Blake, B. G. Heikes, and J. Snow, Evidence from the southern Pacific troposphere for large global abundances and sources of oxygenated organic compounds, *Nature*, *410*, 1078–1081, 2001.

Solberg, S., C. Dye, N. Schmidbauer, A. Herzog, and R. Gehrig, Carbonyls and nonmethane hydrocarbons at rural European sites from the Mediterranean to the Arctic, *J. Atmos. Chem.*, *25*, 33–66, 1996.

Spivakovsky, C. M., et al., Three-dimensional climatological distribution of tropospheric OH: Update and evaluation, *J. Geophys. Res.*, *105*, 8931–8980, 2000.

Wang, Y., D. J. Jacob, and J. A. Logan, Global simulation of tropospheric O_3–NO_x-hydrocarbon chemistry, 1, Model formulation, *J. Geophys. Res.*, *103*, 10,713–10,726, 1998a.

Wang, Y., J. A. Logan, and D. J. Jacob, Global simulation of tropospheric O_3–NO_x-hydrocarbon chemistry, 2, Model evaluation and global ozone budget, *J. Geophys. Res.*, *103*, 10,727–10,756, 1998b.

Warneke, C., T. Karl, H. Judmaier, A. Hansel, A. Jordan, W. Lindinger, and P. J. Crutzen, Acetone, methanol, and other partially oxidized volatile organic emissions from dead plant matter by abiological processes: Significance for atmospheric HO_x chemistry, *Global Biogeochem. Cycles*, *13*, 9–17, 1999.

Wennberg, P. O., et al., Hydrogen radicals, nitrogen radicals, and the production of ozone in the middle and upper troposphere, *Science*, *279*, 49–53, 1998.

Wild, O., X. Zhu, and M. J. Prather, Fast-J: Accurate simulation of in- and below-cloud photolysis in tropospheric chemical models, *J. Atmos. Chem.*, *37*, 245–282, 2000.

Wofsy, S. C., S.-M. Fan, D. R. Blake, J. D. Bradshaw, S. T. Sandholm, H. B. Singh, G. W. Sachse, and R. C. Harriss, Factors influencing atmospheric composition over subarctic North America during summer, *J. Geophys. Res.*, *99*, 1887–1898, 1994.

Wohlfrom, K.-H., T. Hauler, F. Arnold, and H. Singh, Acetone in the free troposphere and lower stratosphere: Aircraft-based CIMS and GC measurements over the North Atlantic and a first comparison, *Geophys. Res. Lett.*, *26*, 2849–2852, 1999.

Wollenhaupt, M., S. A. Carl, A. Horowitz, and J. N. Crowley, Rate coefficients for reaction of OH with acetone between 202 and 395 K, *J. Phys. Chem. A*, *104*, 2695–2705, 2000.

Yokouchi, Y., H. Akimoto, L. A. Barrie, J. W. Bottenheim, K. Anlauf, and B. T. Jobson, Serial gas chromatographic/mass spectrometric measurements of some volatile organic compounds in the Arctic atmosphere during the 1992 Polar Sunrise Experiment, *J. Geophys. Res.*, *99*, 25,379–25,389, 1994.

Zhou, X., and K. Mopper, Apparent partition coefficients of 15 carbonyl compounds between air and seawater and between air and freshwater: Implications for air-sea exchange, *Environ. Sci. Technol.*, *24*, 1864–1869, 1990.

Zhou, X., and K. Mopper, Carbonyl compounds in the lower marine troposphere over the Caribbean Sea and Bahamas, *J. Geophys. Res.*, *98*, 2385–2392, 1993.

Zhou, X., and K. Mopper, Photochemical production of low-molecular-weight carbonyl compounds in seawater and surface microlayer and their air-sea exchange, *Mar. Chem.*, *56*, 201–213, 1997.

I. Bey, B. D. Field, D. J. Jacob, E. M. Jin, Q. Li, J. A. Logan, and R. M. Yantosca, Division of Engineering and Applied Sciences, Department of Earth and Planetary Science, Harvard University, Pierce Hall, 29 Oxford St., Cambridge, MA 02138, USA. (bey@io.harvard.edu; djj@io.harvard.edu; qli@io.harvard.edu; jal@io.harvard.edu)

H. B. Singh, NASA Ames Research Center, Mail Stop 245-5/130, Moffett Field, CA 94035, USA. (hsingh@mail.arc.nasa.gov)